https://doi.org/10.15407/ufm.20.04.634

Yu.F. IVANOV[1], V.E. GROMOV[2], D.V. ZAGULYAEV[2], S.V. KONOVALOV[3], Yu.A. RUBANNIKOVA[2], and A.P. SEMIN[2]

[1] Institute of High-Current Electronics, SB RAS,
2/3 Akademicheskiy Ave., 634055 Tomsk, Russia

[2] Siberian State Industrial University,
42 Kirov Str., 654007 Novokuznetsk, Russia

[3] Academician S. P. Korolyov Samara National Research University,
34 Moskovskoye Shosse, 443086 Samara, Russia

THE STRUCTURE AND PROPERTIES OF A HYPOEUTECTIC SILUMIN SUBJECTED TO COMPLEX ELECTRON–ION-PLASMA PROCESSING

The layer-by-layer analysis of structural–phase states and tribological properties of hypoeutectic AK10M2H-type silumin at the depth up to 170 μm after the complex processing is carried out by the state-of-the-art methods of physical materials science. It involves the electroexplosion alloying with titanium and yttrium-oxide powder in different ratios followed by electron-beam processing. The choice of titanium and yttrium as the alloying elements is caused by the fact that, at the solidification, they form the eutectic mixture of two restricted solid solutions. Four variants of the combined surface treatment are realized in the work: the masses of the exploded titanium foil and Y_2O_3 powder are 58.9 mg each at the electron-beam energy density E_s = 25 J/cm^2 and discharge voltage U = 2.8 kV as well as 58.9 and 88.3 mg at E_s = 35 J/cm^2 and U = 2.6 kV. As revealed, the electroexplosion treatment is accompanied with both the alloying of the surface layer with plasma elements and the penetration of the initial powder particles of yttrium oxide into the surface layer. The complex surface processing leads to the dissolution of Si inclusions and intermetallides typical for the cast state. Depending on the regime, the complex surface treatment forms the multicomponent multiphase layer of the thickness of up to ≈170 μm; the crystallites' sizes of the layer vary within the range from units to hundreds of nanometers. Along with the atoms of the initial material (Al, Si, Cu, Ni, Fe), the surface layer is enriched by the atoms of titanium, yttrium, oxygen. The inhomogeneous distribution of the alloying elements in the modified layer is determined by the method of mapping. As found out, the modified layer has the structure of high-velocity cellular crystallization and contains the inclusions of the faceted form,

whose relative content decreases as moving away from the surface. The cells of high-rate crystallization are enriched mainly with Al atoms; the interlayers separating the cells are mostly enriched with Si atoms; the inclusions of faceted form are mostly enriched with Ti, Al, and Cu atoms; Y atoms form mainly the interlayers over the boundaries of faceted-form inclusions. As detected, silicon interlayers located over the boundaries and in the junctions of cell-crystallization boundaries formed by the Al-based solid solution have a nanocrystalline structure with crystallites' sizes varying within the range of 10–20 nm. The complex surface processing increases the wear resistance by 18–20 times with respect to the initial silumin, and 2.6–2.8 times with respect to the silumin after the electroexplosion alloying. The friction coefficient increases by ≈1.5 times with respect to the initial silumin.

Keywords: hypoeutectic silumin, electroexplosion alloying, titanium, yttrium, electron beam processing, structure, phase composition, wear resistance.

1. Introduction

The modification of the surface properties of light metals and alloys is not only widely investigated but still a rather promising direction. The operation efficiency of the surface hardened product is determined by many factors the main of which are: strength and hardness of the strengthened zone, homogeneity of structure and properties, high resistance to failure, mainly, crack initiation. In recent years, the impact of the studies in the field of physical material science is focused on the clarification of the nature of the increase in the properties of metals and alloys at the expense of the processing by the concentrated fluxes of energy [1]. Among the variety of the methods of surface modification (laser, plasma, ultrasonic processing, ion beams *etc.*) the electroexplosion alloying (EEA) [2] and electron beam processing (EBP) hold the special position [3, 4]. The important feature of EEA consists in the fact that the source of the alloying elements is a multiphase jet of explosion itself and the results are determined by the mutual action of the heat, power and chemical factors of effect on the surface. It permits one to perform the alloying both by simple metals and complex compounds — carbides, oxides, borides *etc.*, ensuring the high level of service properties of the surface [5–10]. The simultaneous occurrence of a series of interconnected processes determining the formation of new structural phase states and properties of the surface layers at EEA poses a problem of full-scale determination of its possibilities and control of its results, the development of specialized equipment with high level of mechanization and automatization of the process [11].

In comparison with the other types of modifications of material's surface, the low-energy (<30 keV) electron beams are generated with a substantially higher efficiency (<90%) in frequency-pulsed (up to ≈10 Hz) regime at a lesser (by an order of magnitude) accelerating voltage. These beams require no a special radiation protection, because the ac-

companying x-ray radiation is shielded by the walls of the working vacuum chamber. The high-energy efficiency, higher homogeneity of energy density by flux cross-section, good reproducibility of pulses and high pulse repetition rate distinguish favourably the pulsed electron beams from the pulsed fluxes of low-temperature plasma in the potential application of them in technological purposes as well. The EBP possesses the higher possibilities of the supplied energy control, the creation of large area of effect of concentrated energy flux on the processed material, the small energy reflection coefficient, the high-energy concentration in the volume unit of the material. The EBP provides the super-high speeds of heat (up to 10^6 K/s) of the surface layer, the formation of the limiting by magnitude gradients of temperature (up to 10^7–10^8 K/m), and the cooling of the surface layer due to the heat removal to the main volume of the material at speeds of 10^4–10^9 K/s. As a result, the conditions of the formation of nonequilibrium submicro- and nanocrystalline and amorphous structural phase states [12–13] are created in the surface layer.

At energy density of electron beam of ≤3 J/cm^2 the equilibrium fine grained structure several micrometers thick is formed in eutectic and hypereutectic silumin, the dissolution of silicon particles in aluminium matrix is observed, the supersaturated solid solution in the molten layer is formed [14–24]. The increase in the energy density of electron beam to 10–35 J/cm^2 results in the more cardinal change in structural phase states and tribological properties of hypoeutectic silumin [25–29].

The EBP at energy density of 25–30 J/cm^2 results in the melting of the surface layer, the dissolution of silicon inclusions and intermetallides, the formation of the structure of high strength cellular crystallization, the repeated precipitation of the second phase particles of submicro–nanoscale ranges. The multiple changes in the mechanical and tribological characteristics of the silumin surface layer irradiated by the pulsed electron beam of this density have been found. It has been shown that the friction coefficient decreases by 1.3 times, the parameter of wear (the value reverse to wear resistance) — by 7 times, the microhardness increases by 1.7 times. It has been suggested that the increase in the wear resistance of silumin modified layer by 7 times with respect to the cast state is caused by the formation of submicro–nanoscale multiphase structure of cellular crystallization free from usual inclusions of silicon and intermetallides [25–29].

The EEA and EBP are well combined with each other, have the correlated values of pulse time, diameter of the irradiated surface, intensity and depth of the effect zone. At the same time the electron beam processing exerts no pressure on the surface. Resulting in its melting it smooths the relief under the action of capillary forces. It is not the only

reason attracting interest to the combined treatment uniting EEA followed by the electron beam effect. That type of treatment results in the change in the structural phase states and improvement of surface layer properties [30–34].

In Ref. [34] the studies of Ti–Y alloy structure being formed in the substantially nonequilibrium conditions of high velocity crystallization realized upon combined treatment uniting the electroexplosion alloying of titanium by yttrium and the subsequent irradiation of the modified surface by the intense pulsed electron beam of microsecond duration of effect have been carried out. The formation of the cellular crystallization structure presented by yttrium grains of submicron (150–300 nm) sizes surrounded by titanium interlayers of nanodimensional (≈100 nm) thickness has been revealed in the surface layer of titanium. Based on the performed examinations, it has been suggested that the formation of submicro–nanoscale structure is caused by the combined action of two factors: the high speed of cooling of the melt and the presence of the elements practically insoluble in each other in the solid state [34]. Titanium and yttrium were used as the alloying elements in this research. The Ti–Y system belongs to the binary system with the restricted solubility having no intermetallic compounds [35, 36]. According to the equilibrium diagram, yttrium and titanium are completely mixed in the liquid state, but on solidification, they form the eutectic mixture of two restricted solid solutions [35, 36]. In the solid state (lower than temperature of 875 °C), the material is presented by the mixture of two phases: α-Ti and α-Y.

The goal of the present study is to analyse the results and to reveal the regularities of evolution of the elemental and phase composition, the state of the defect substructure of hypoeutectic АК10М2Н-type silumin subjected to the combined treatment. The treatment consists in two stages: the first stage includes the electroexplosion alloying of the material's surface, and at the second one — the irradiation of the alloyed layer by intense pulsed electron beam.

2. Material and Study Methods

The АК10М2Н-grade silumin in the cast state (permanent-mould casting) was used as the material under study. The chemical composition of АК10М2Н silumin is given in Table 1 [37]. The samples had the form of plates with sizes of $20 \times 20 \times 15$ mm^3.

The surface modification of silumin samples was performed by the combined method uniting the electroexplosion alloying (the first stage of the processing [2]) and the irradiation by the intense pulsed electron beam (the second stage of the processing [13]). The electroexplosion alloying was carried out with yttrium oxide powder located on the VT1-0

titanium foil (the regimes of electroexplosion alloying are given in Table 2).

The irradiation of silumin sample by intense pulsed electron beam was carried out at the SOLO plant [38]. The electron beam parameters: the energy of accelerated electron U = 17 keV; the energy density of electron beam E_s = 25 J/cm^2 and E_s = 35 J/cm^2; the pulse duration τ = = 150 μs; the pulse number n = 3; the pulse repetition rate f = 0.3 s^{-1}; the pressure of residual gas (argon) in the working chamber of the plant $p = 2 \cdot 10^{-2}$ Pa. The irradiation parameters chosen based on the results of temperature field modelling formed at EBP [39–42].

Thus, the following four variants of the combined treatment of АК10М2Н silumin were realized: variant 1 — EEA (mode 1) + EBP (E_S = = 25 J/cm^2); variant 2 — EEA (mode 1) + EBP (E_S = 35 J/cm^2); variant 3 — EEA (mode 2) + EBP (E_S = 25 J/cm^2); variant 4 — EEA (mode 2) + + EBP (E_S = 35 J/cm^2).

The studies of the elemental and phase composition, the state of defect substructure were carried out by the methods of scanning electron microscopy (device Philips SEM-515), transmission electron diffraction microscopy (device JEM-2100F) [43–45]. The foils manufactured by the methods of ion thinning of plates cut out perpendicular to the surface of irradiation were analysed. This location of foils enables the structure and elemental composition of the material to be analysed depending on the distance from the surface of modification. The elemental composition of the material was studied by the methods of micro-x-ray spectral analysis. The tribological studies (the determination of wear resistance and friction coefficient) were performed at tribometer Pin on Disc and Oscillating TRIBOtester (TRIBOtechnic, France) at the following parameters: the ball made of ball bearing steel 6 mm in

Table 1. **Chemical composition of АК10М2Н silumin according to the State Standard (GOST) 30620-98 in percentage. Al acts as a base component**

Fe, %	Si, %	Mn, %	Ni, %	Ti, %	Al, %	Cu, %	Pb, %	Mg, %	Zn, %	Sn, %	Impurities, %
≤0.6	9.5–10.5	≤0.05	0.8–1.2	≤0.05	≈84.28–86.1	2–2.5	≤0.05	0.9–1.2	≤0.06	≤0.01	total 0.7

Table 2. **Electroexplosion alloying modes (regimes) for АК10М2 silumin**

No. of mode	Mass of Ti foil, m_{Ti}, g	Mass of Y_2O_3 powder, $m_{Y_2O_3}$, g	Discharge voltage, U, kV
1	0.0589	0.0589	2.8
2	0.0589	0.0883	2.6

diameter, the track radius — 4 mm, the indenter load and track length varied depending on the level of wear resistance of the material. The degree of wear was determined by the results of profilometry of track formed in tests.

3. Results and Discussion

3.1. Structure of AK10M2H Silumin in the Cast State

Al–Si alloy (hypoeutectic silumin), being the material under study, contains a relatively large set of alloying and impurity elements (Table 1). The presence of the alloying and impurity elements contributes to, on the one hand, the increase in the strength properties of the material, but, on the other hand, results in the decrease in crack resistance of silumin that is caused by the formation of silicon and intermetallides of lamellar morphology [13, 37, 38, 46]. The characteristic images of the etched metallographic section structure of silumin under study obtained

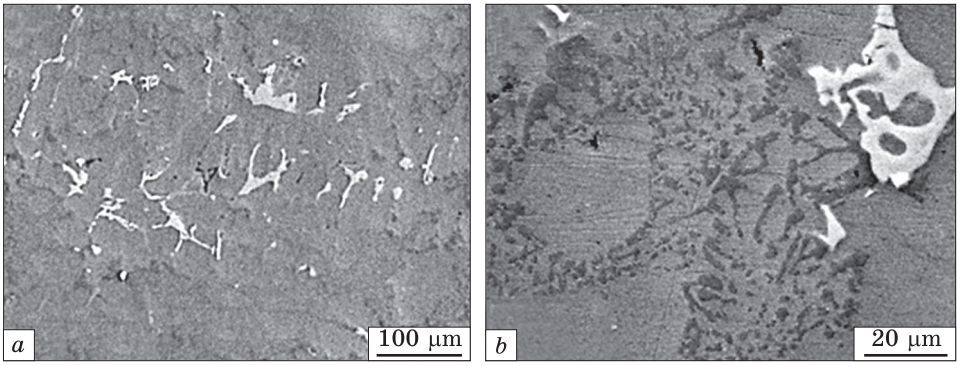

Fig. 1. Silumin structure in the cast state observed *via* the scanning electron microscopy (SEM).

Table 3. **Results of micro-x-ray spectral analysis of the surface areas of silumin sample. The electron-microscopic image of the sample is presented in Fig. 2**

Area	Element (balance Al, wt.%)				
	Si	Ni	Cu	Fe	Mn
1	0.6	13.5	13.3	0.0	0.0
2	8.7	0.3	2.2	0.0	0.0
3	1.7	11.8	14.0	0.0	0.0
4	0.5	0.2	1.3	0.0	0.0
5	22.5	1.1	1.6	1.2	0.0
6	1.1	14.8	15.8	0.5	0.0
7	2.3	17.2	5.2	2.7	0.6

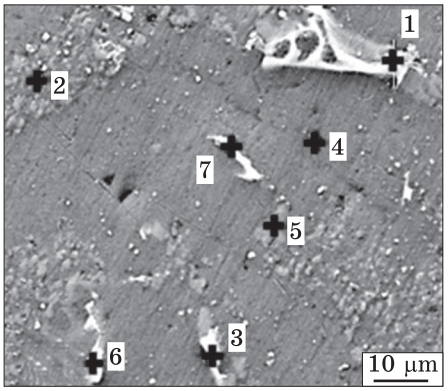

Fig. 2. SEM image of silumin structure, where the designations show the areas wherein the micro-x-ray spectral analysis of elemental composition was made

by the methods of scanning electron microscopy and demonstrating the monophase, morphologically varied character of the material are presented in Fig. 1.

The inclusions of the second phases have various shapes. Their sizes vary within the limits of units — tens of micrometers. According to the metallographic studies [46–49], using the methods of the selective etching, one can reveal in silumins as follows. The lamellar inclusions of the light-grey colour — β-phase Al_5SiFe; the inclusions having the shape of symmetrical polyhedron of the brown colour — α-phase $Al_{15}(FeMn)_3Si_2$ with small quantity of iron particles' shape similar to the Chinese hieroglyphs; the grey-colour inclusions of the oval shape are silicon particles.

The elemental composition of different areas in the cast silumin was examined by the methods of micro-x-ray spectral analysis (Fig. 2). The results of the examinations presented in Table 3 are indicative of the fact that the chemical elements of the alloy are distributed rather non-uniformly in the bulk of the material and they form the compounds being distinguished in the sizes, contrast, morphology and elemental composition. It is interesting to note that the relative content of copper and nickel is higher in the grain of Al–Si (area 2 in Fig. 2) eutectic than in aluminium grain (area 4 in Fig. 2).

Thus, the performed studies have revealed the formation of the multiphase structure containing the inclusions of silicon and intermetallides of various shapes whose sizes reach tens of micrometers.

3.2. Structure of Silumin after the Combined Treatment

3.2.1. Variant 1: EEA (mode 1) + EBP (E_s = 25 J/cm^2)

The characteristic electron microscopic images of silumin surface structure subjected to the combined treatment are presented in Fig. 3. The presence of a large number of microcraters (Fig. 3, *a*, *b*, microcraters are designated by the arrows) and the particles of droplet fraction (Fig. 3, *c*, where arrows designate the particles) is clearly seen. The formed surface layer is separated into areas whose sizes are less than 1 μm (Fig. 3, *d*). The areas have a polycrystalline structure; the crystallites' sizes vary within the limits from 60 nm to 100 nm (Fig. 3, *d*, the inset).

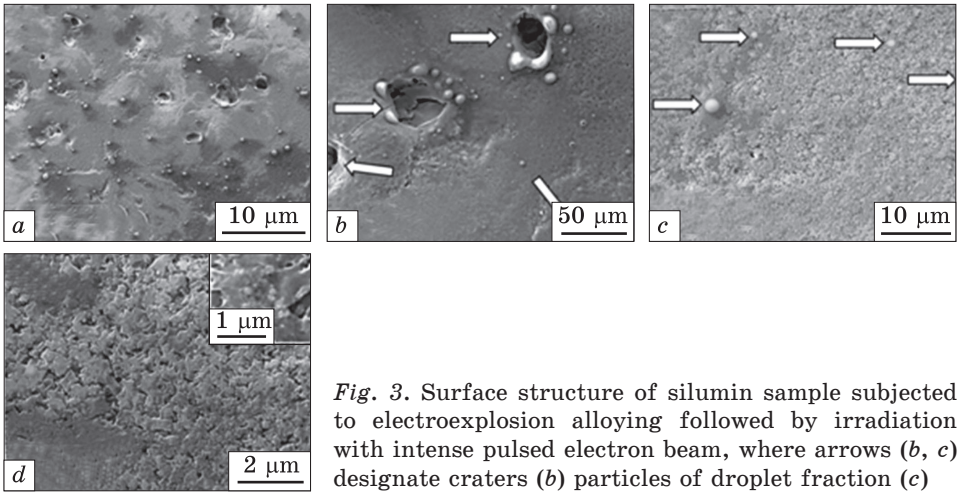

Fig. 3. Surface structure of silumin sample subjected to electroexplosion alloying followed by irradiation with intense pulsed electron beam, where arrows (*b*, *c*) designate craters (*b*) particles of droplet fraction (*c*)

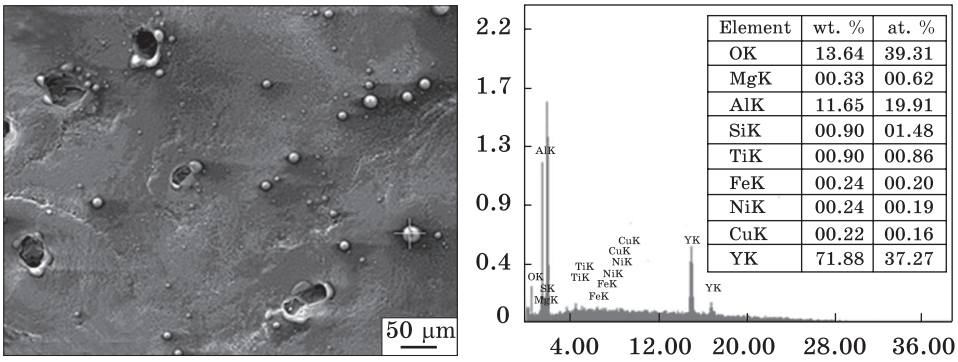

Element	wt. %	at. %
OK	13.64	39.31
MgK	00.33	00.62
AlK	11.65	19.91
SiK	00.90	01.48
TiK	00.90	00.86
FeK	00.24	00.20
NiK	00.24	00.19
CuK	00.22	00.16
YK	71.88	37.27

a *b*

Fig. 4. Structure (*a*) and energy spectra (*b*) obtained *via* the micro-x-ray spectral analysis of microdroplet designated (+) in (*a*). Here, complex modification corresponds to variant 1

The elemental composition of silumin surface layer modified according to variant 1 was studied by the methods of micro-x-ray spectral analysis. The results of the performed studies have shown that the average concentration of titanium atoms amounts to 17.6 wt.%, yttrium — 14.3 wt.%, oxygen — 6.7 wt.% in the surface layer. The concentration of yttrium and oxygen atoms in the particles of droplet fraction is substantially higher (Fig. 4).

The structure and elemental composition of the surface layer of the modified silumin were studied by examination of transverse metallographic sections. Analysing results in Fig. 5, we can note that the thickness of the modified layer varies within the range 50–70 μm. The mod-

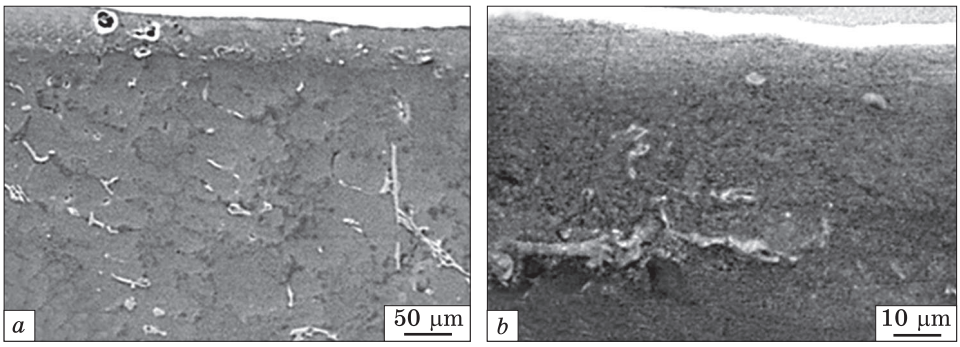

Fig. 5. Characteristic electron microscopic image for transverse metallographic section of silumin subjected to combined treatment including electroexplosion alloying and subsequent irradiation by intense pulsed electron beam

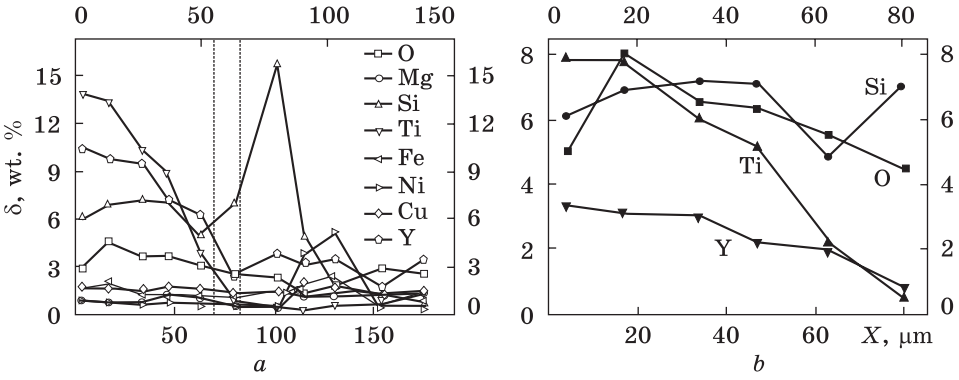

Fig. 6. Dependence of distribution of relative content of elements on distance from the silumin-modified layer (SEM method)

ified layer has a submicrocrystalline structure and is free from the inclusions of silicon and intermetallides being present in the bulk of the samples.

The studies on the atoms' distribution of silumin chemical elements in the thickness of the modified layer were carried out using the methods of micro-x-ray spectral analysis. The results in Fig. 6 show that the maximum concentration of titanium, yttrium, and oxygen introduced additionally into the alloy concentrated in the surface layer of the sample 70–80 μm thick. When moving away from the surface of modification, the concentration of these elements decreases. The modified layer is characterised by the uniform distribution of the chemical elements. Beyond this layer, the areas with the increased content of some elements (*e.g.*, silicon, nickel, iron and copper) (Fig. 6, *a*) are present. It should be noted that titanium concentration in the modified layer is substantially higher than that of yttrium as well.

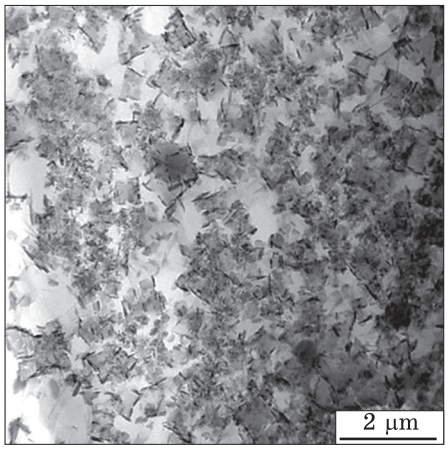

Fig. 7. Electron microscopic image of the structure of silumin surface layer modified within the framework of variant 1

Thus, the complex treatment combining the electroexplosion alloying of silumin by titanium and yttrium oxide and the subsequent irradiation by intense pulsed electron beam at energy density of electron beam of 25 J/cm^2 is accompanied with the formation of the modified layer up to 70 μm thick enriched by atoms of titanium, yttrium, and oxygen. The elemental and phase composition, the defect substructure of silumin subjected to the combined surface treatment were studied by the methods of transmission electron diffraction microscopy (TEDM). For this purpose, the foils making it possible to analyse the change in the elemental composition and structural phase state of the material depending on the distance from the surface of modification were fabricated from the plates cut out perpendicular to the surface of modification from the massive sample by the methods ion thinning. The characteristic image of surface layer structure obtained by scanning electron microscopy method is shown in Fig. 7. As clearly seen, the modified layer is formed by the crystallites of different morphology whose sizes vary in the submicro–nanoscale range.

The results of the elemental composition study of silumin surface layer subjected to the combined treatment are shown in Fig. 8. The size of the foil volume under study were 9.5×9.5×0.3 μm. Analysis of the results presented in this figure shows that the thickness of silumin layer alloyed with Y, O, and Ti amounts of 60–70 μm. At the larger distance from the surface of modification, the concentration of these elements was negligibly small.

The elemental composition of the modified layer depends on the distance from the surface of treatment. The concentration of O and Y atoms decreases the most substantially with moving away from the surface of treatment.

The main alloying element of the modified layer is titanium whose concentration in the layer on the average amounts to ≈11 at.% and varies in the limits of 9–14.5 at.% showing the tendency to the increase with moving away from the surface of alloying. The relative content of yttrium and oxygen decreases monstrously with the growth of distance from the surface of alloying.

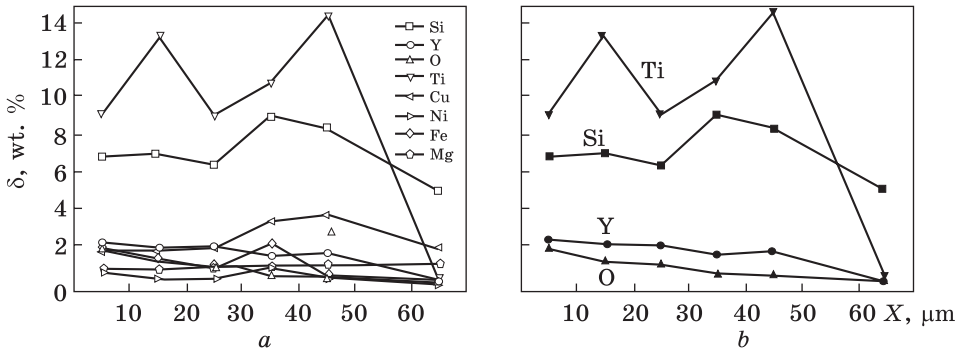

Fig. 8. Concentration of chemical elements (excluding Al) in silumin subjected to complex treatment (variant 1) *vs*. distance from surface of modification (SEM method)

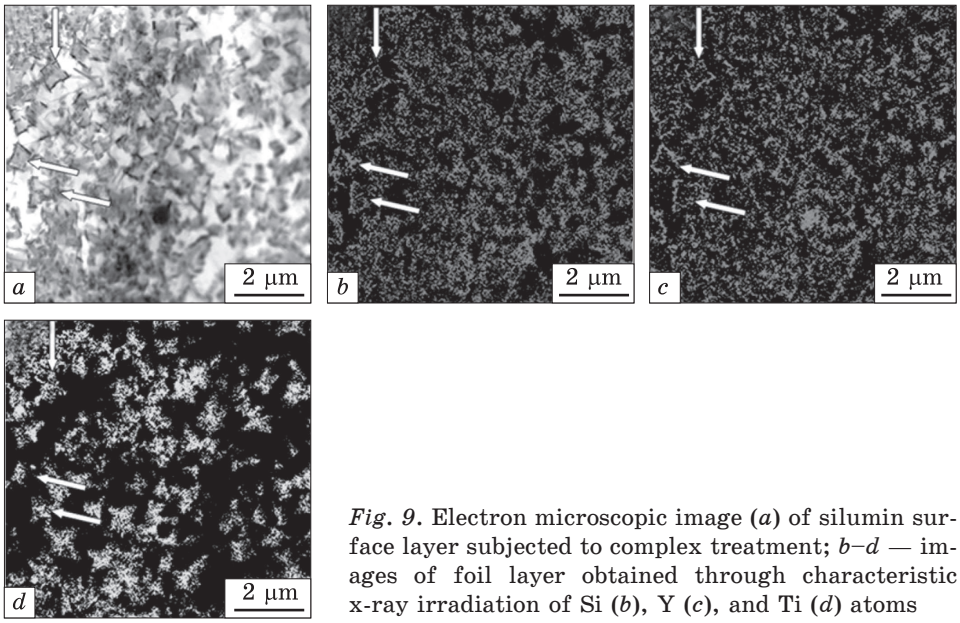

Fig. 9. Electron microscopic image (*a*) of silumin surface layer subjected to complex treatment; *b*–*d* — images of foil layer obtained through characteristic x-ray irradiation of Si (*b*), Y (*c*), and Ti (*d*) atoms

The distribution of the alloying elements in the modified layer was studied using the mapping methods [50]. The results of mapping of surface layer 10 μm thick are shown in Fig. 9. The results of the quantitative analysis of the elemental composition of the layer are presented in Table 4 (layer 0–10 μm).

It is clearly seen that the main element of the layer under study is aluminium. The principal elements alloying aluminium are titanium, silicon, yttrium, oxygen, and copper. These elements are distributed nonuniformly in this layer forming the inclusions of different shapes of submicron sizes (Fig. 9, the inclusions are designated by arrows).

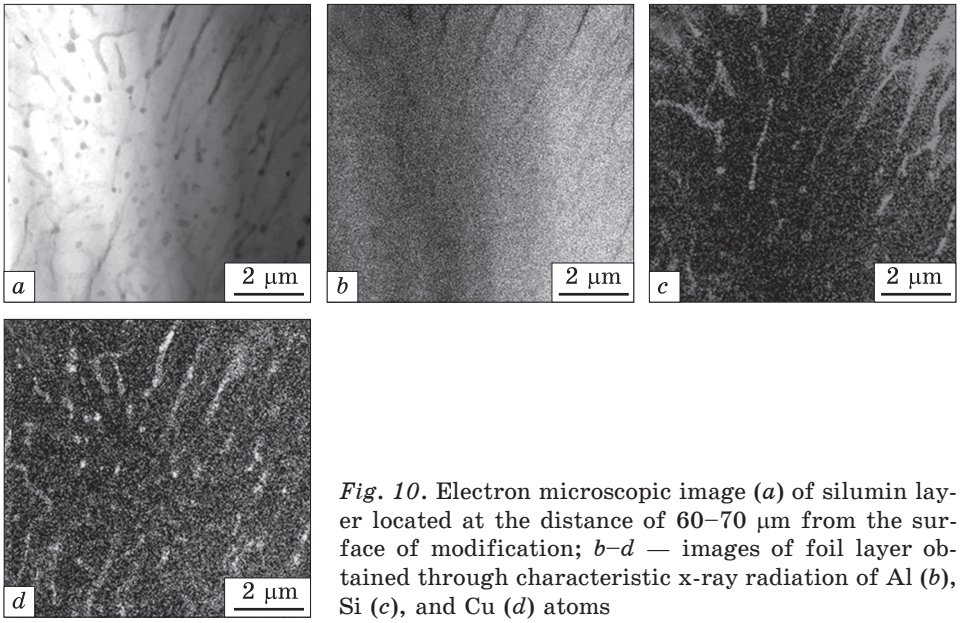

Fig. 10. Electron microscopic image (*a*) of silumin layer located at the distance of 60–70 μm from the surface of modification; *b–d* — images of foil layer obtained through characteristic x-ray radiation of Al (*b*), Si (*c*), and Cu (*d*) atoms

The bulks of inclusions are enriched with Ti atoms, the atoms of Y and Si form the envelope of these inclusions. In some cases, the atoms of Cu are present in the envelope. The similar structure is revealed in the layer of ≈60 μm thick. At the larger distance from the modified surface, the structure of high-velocity cellular crystallization whose main alloying elements are Si and Cu (Fig. 10) is observed.

The cells' volume is formed by the Al-based solid solution (Fig. 10, *b*), the extended interlayers enriched by the Si and Cu atoms (Fig. 10, *c*, *d*) are located at the boundaries of cells. The thickness of these interlayers varies within the 50–250 nm. At the larger distance from the surface of modification, the structure characteristic of the cast silumin detected the grains of solid solution based on aluminium, the eutectics, and the inclusions of silicon and intermetallides of various elemental compositions.

Table 4. **Chemical composition (at.%) of silumin layers located at different distances (*X*) from the surface subjected to complex treatment**

X, μm	Al	Si	Y	O	Ti	Cu	Ni	Fe
0–10	76.03	6.77	2.26	1.73	9.10	1.72	0.45	1.94
10–20	73.00	7.01	1.99	1.15	13.37	1.79	0.32	1.36
20–30	78.71	6.35	2.01	1.00	9.03	1.88	0.29	0.72
30–40	72.03	9.00	1.42	0.42	10.84	3.34	0.80	2.15
40–50	70.73	8.36	1.59	0.43	14.60	3.70	0.16	0.42
60–70	92.87	4.88	0.00	0.26	0.06	1.85	0.04	0.04

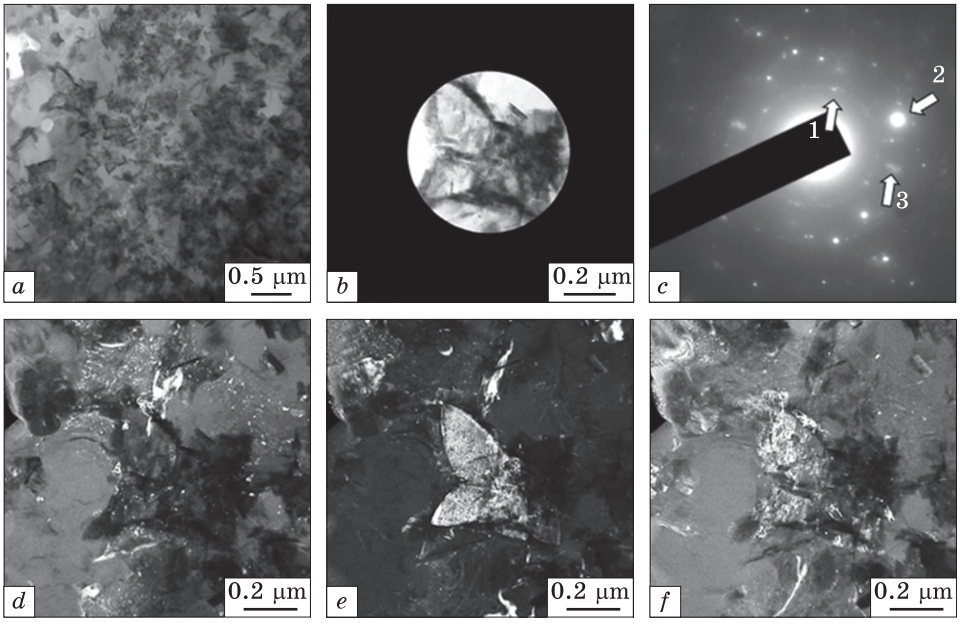

Fig. 11. Electron microscopic image of surface layer structure of silumin subjected to complex treatment under conditions of variant 1. Here, *a*, *b* — bright fields; *c* — microelectron diffraction pattern (the reflections in which dark fields were obtained are designated by arrows: *1* — *d*, *2* — *e*, *3* — *f*); *d*–*f* — dark fields obtained in reflections [111]Si (*d*), [101]α-Ti (*e*), [040]SiY + [103]Cu_2YSi_2 + [210]SiTi (*f*), respectively. Selective diaphragm (*b*) marks out the foil area for which microelectron diffraction pattern was observed

The phase composition of the modified layer has been analysed using the dark-field images of transmission electron-diffraction microscopy and the technique of interpretation of microelectron diffraction patterns [43–45, 51, 52]. The electron microscopic bright-field image of this layer is depicted in Fig. 11.

Microelectron diffraction pattern obtained from the foil's area singled out by selective diaphragm (Fig. 11, *b*) contains a large number of reflections of different intensity (Fig. 11, *c*). The interpretation of the microelectron diffraction pattern enabled to find the reflections of the following phases: silicon, α-titanium, SiY, SiTi, and Cu_2YSi_2. The reflections belonging to the crystal lattice of silicon form the diffraction rings (Fig. 11, *c*, reflection 1) that is indicative of the small sizes of the particles in this phase. Actually, the dark-field image obtained in the reflection of ring [111]Si demonstrates the presence of nanoscale (10–20 nm) particles (Fig. 11, *d*) in the structure of silumin. The most intense reflection of microelectron diffraction pattern (Fig. 11, *c*, reflection 2) corresponds to [101]α-Ti. The dark-field image (Fig. 11, *e*) of foil obtained in this reflection is indicative of the fact that the particles

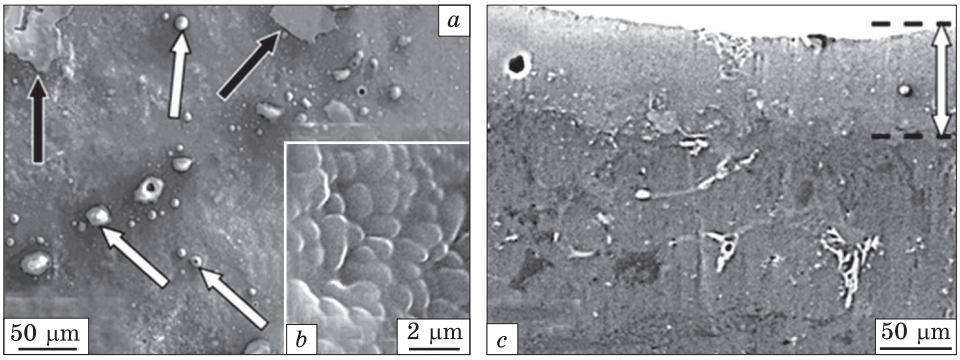

Fig. 12. Structure of silumin sample subjected to electroexplosion alloying and subsequent irradiation by intense pulsed electron beam: *a*, *b* — structure of irradiation surface; *c* — structure of transverse etched metallographic section. Dark and light arrows designate films and droplets (*a*, *b*) located on the surface of the sample, respectively, and modified layer (*c*)

with faceting are formed by α-titanium. The most complicated for interpretation is the dark-field image obtained in closely located reflections designated by 3 in Fig. 11, *c*. The microelectron-diffraction pattern analysis enables one to suggest that these reflections belong to SiY, Cu_2YSi_2, and SiTi phases, which judging by the dark-field image presented in Fig. 11, *f* form the envelope of α-titanium particles.

It is evident that the revealed transformation of silumin surface layer should have a substantial effect on the tribological properties of the material. Actually, the performed tests have shown that the complex surface treatment of silumin leads to the multiple increases (by ≈19.6 times) of the wear resistance of the modified layer and the decrease (by ≈1.5 times) of the friction coefficient caused by the formation of multiphase submicro–nanocrystalline state.

3.2.2. Variant 2: EEA (mode 2) + EBP (E_s = 25 J/cm^2)

The characteristic electron microscopic images of silumin surface structure subjected to the complex treatment according to this mode are shown in Fig. 12, *a*, *b*. It is clearly seen that as a result of the treatment the surface containing the microcraters, microdroplets and the formations of film shape are formed (Fig. 12, *a*). The formed surface layer has a submicrocrystalline structure; the crystallites are less than 1 μm (Fig. 12, *b*). The structure analysis of the etched transverse metallographic sections has shown that the thickness of the layer modified as a result of the complex treatment amounts to 70–80 μm (Fig. 12, *c*).

The elemental composition, phase morphology, state of silumin defect structure at different distance from the surface of treatment were studied by TEDM methods. The analysis of the images presented in

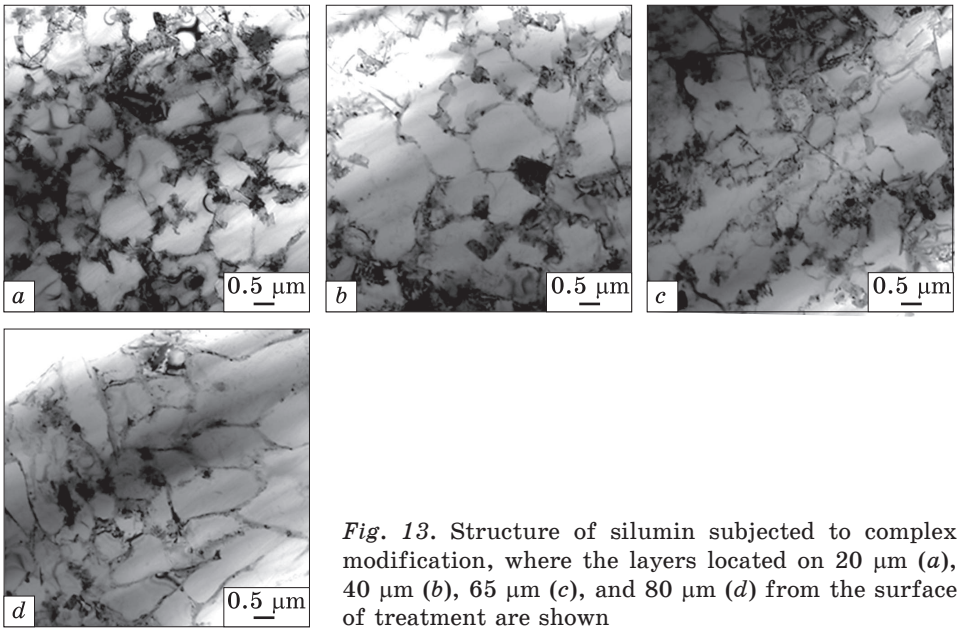

Fig. 13. Structure of silumin subjected to complex modification, where the layers located on 20 μm (*a*), 40 μm (*b*), 65 μm (*c*), and 80 μm (*d*) from the surface of treatment are shown

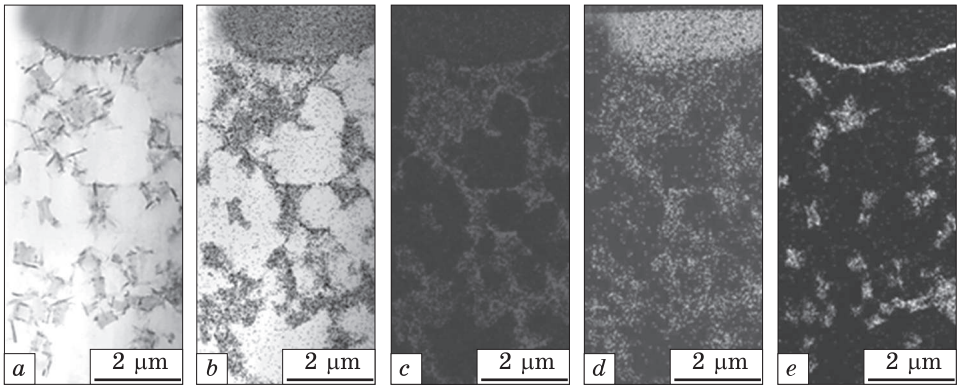

Fig. 14. Electron microscopic image of surface layer structure of modified silumin (*a*) and images of this layer obtained through characteristic x-ray radiation of Si (*c*), Y (*d*), and Ti (*e*) atoms. Image (*b*) obtained by superposition of images (*c*–*e*)

Fig. 13 shows that in the layer up to 80 μm thick the structure of cellular crystallization is formed. The cells' size varies within the limits from 0.8 μm to 1.3 μm. The cells are separated by the interlayers of the second phase. The thickness of the interlayers varies within the limits of 50–75 nm. The inclusions of the second phase having the faceted shape in the form of cuboid or four-petal rosettes are located principally in the triple junction of the cell's boundaries. The sizes of these inclusions vary within the limits of 0.5–0.7 μm. Thus, the complex

treatment according to the second variant results in the formation of the surface layer whose second phase inclusions are repeatedly less (by tens–hundreds of times) than the inclusions being present in silumin of cast state.

The distribution of chemical elements in the modified layer was studied by the methods of micro-x-ray spectral analysis of thin foils. The results of elemental analysis (method of mapping [50]) of the layer adjoining to the surface of modification are shown in Fig. 14. As clearly seen, the interlayers located at the boundaries of high-velocity crystallization cells are enriched by silicon and yttrium atoms. Titanium atoms are enriched by the particles of the faceted shape. The yttrium atoms form the thin films and droplets located on the surface of sample's modification.

In a quantitative ratio the elemental composition of the surface layer whose image is presented in Fig. 14, *a*, is listed in Table 5. Analysing the results of the table, we can noted that the principal chemical element of the layer under study is aluminium the mass fraction of which is more than 75%. The concentration of the revealed alloying elements varies within the limits from 1 to 5 mas.%.

The elemental composition of the modified layer detected by the methods of electron microscopy of thin foils depends on the distance from the surface of treatment as follows from the results presented in Fig. 15. The concentration of O and Ti atoms decreases the most substantially with move away from the surface of treatment.

Using the dark-field images and the technique of microelectron-diffraction pattern interpretation [43–45, 51, 52] by the methods of

Table 5. **Chemical composition of silumin surface layer (see image in Fig. 14, *a*) subjected to complex treatment according to variant 2**

Thin film	Standardless	Standardless	Quantitative analysis		
Fitting coefficient: 0.1703			counts	error, %	at.%
Element	keV	mas.%			
O	0.525	2.30	10875.08	0.11	4.17
Mg	1.253	1.13	9213.72	0.20	1.35
Al	1.486	75.76	626449.69	0.00	81.60
Si	1.739	5.01	43060.93	0.05	5.18
Ti	4.508	5.14	33403.07	0.06	3.12
Fe	6.398	2.49	13508.27	0.16	1.30
Ni	7.471	1.07	5163.90	0.48	0.53
Cu	8.040	3.33	14151.06	0.19	1.52
Y	1.922	3.78	8101.01	0.34	1.23
Total		100.00			100.00

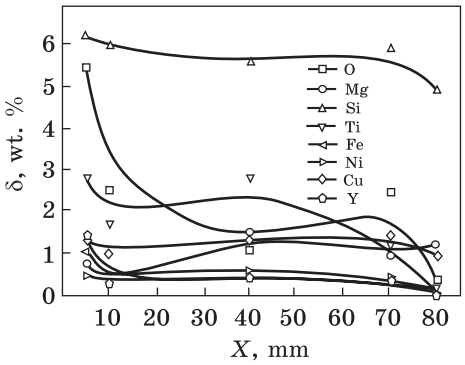

Fig. 15. Concentration of chemical element (excluding Al) in silumin (subjected to complex treatment (variant 2) *vs*. distance from the surface of modification

transmission electron-diffraction microscopy the analysis of phase composition of the modified layer was carried out. Figure 16, *a* shows the electron microscopic bright-field image of the surface layer of modified silumin. The microelectron diffraction pattern obtained from the foil's part singled out by selective diaphragm (Fig. 16, *b*) contains the diffraction halo corresponding to the amorphous state of the substance and the reflection forming the diffraction rings (Fig. 16, *c*). The microelectron-diffraction pattern analysis enabled the reflections of silicon and SiY yttrium silicide to be revealed. Following the results of micro-x-ray spectral analysis of the foil's part presented in Fig. 16, *d*, it can be supposed that the amorphous phase is the region of sample's surface (film or droplet) enriched by yttrium. One of the phases possessing a nanocrystalline structure and locating along droplet (main volume of sample interface) is SiY yttrium silicide.

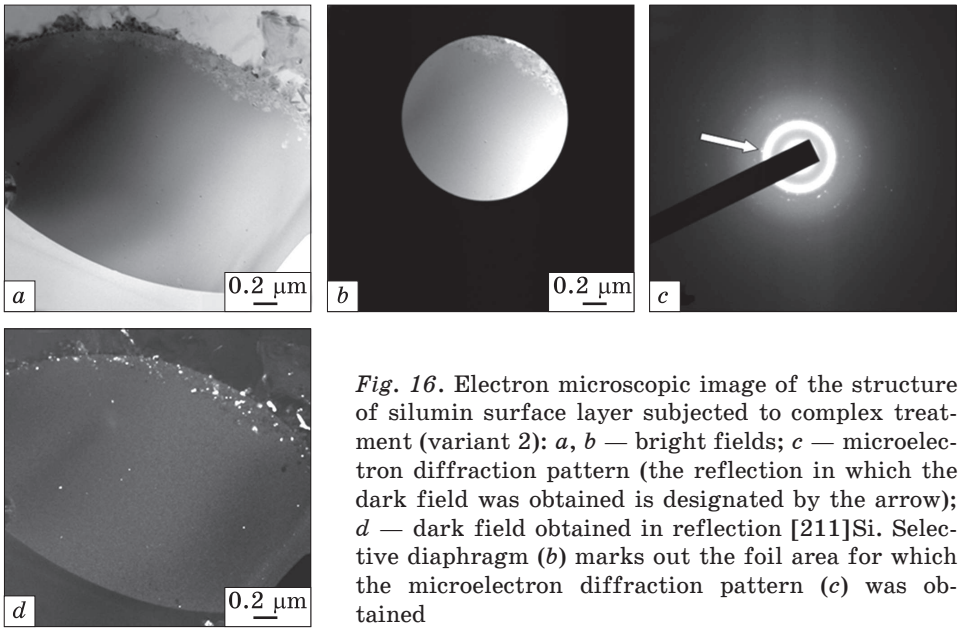

Fig. 16. Electron microscopic image of the structure of silumin surface layer subjected to complex treatment (variant 2): *a*, *b* — bright fields; *c* — microelectron diffraction pattern (the reflection in which the dark field was obtained is designated by the arrow); *d* — dark field obtained in reflection [211]Si. Selective diaphragm (*b*) marks out the foil area for which the microelectron diffraction pattern (*c*) was obtained

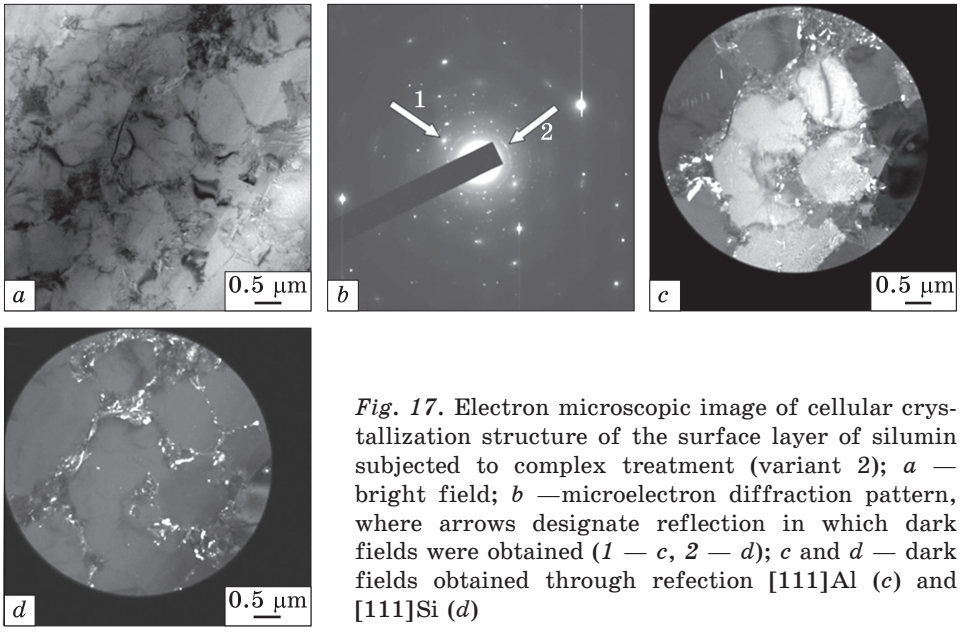

Fig. 17. Electron microscopic image of cellular crystallization structure of the surface layer of silumin subjected to complex treatment (variant 2); *a* — bright field; *b* —microelectron diffraction pattern, where arrows designate reflection in which dark fields were obtained (*1* — *c*, *2* — *d*); *c* and *d* — dark fields obtained through refection [111]Al (*c*) and [111]Si (*d*)

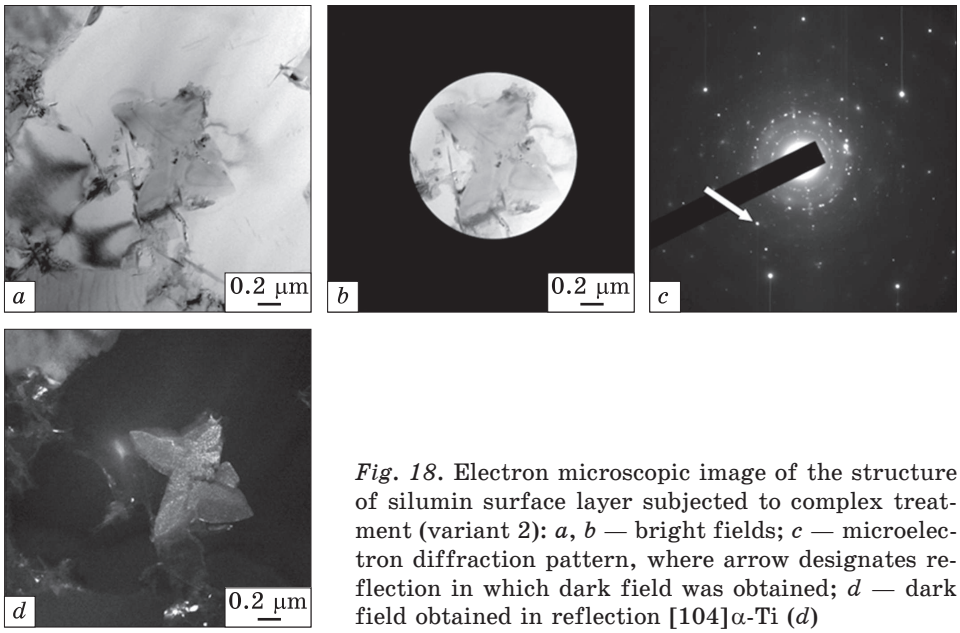

Fig. 18. Electron microscopic image of the structure of silumin surface layer subjected to complex treatment (variant 2): *a*, *b* — bright fields; *c* — microelectron diffraction pattern, where arrow designates reflection in which dark field was obtained; *d* — dark field obtained in reflection [104]α-Ti (*d*)

Electron microscopic image of cellular crystallization structure of the modified layer is shown in Fig. 17. It is clearly seen that the volume of high-velocity crystallization cells is formed by the solid solution based

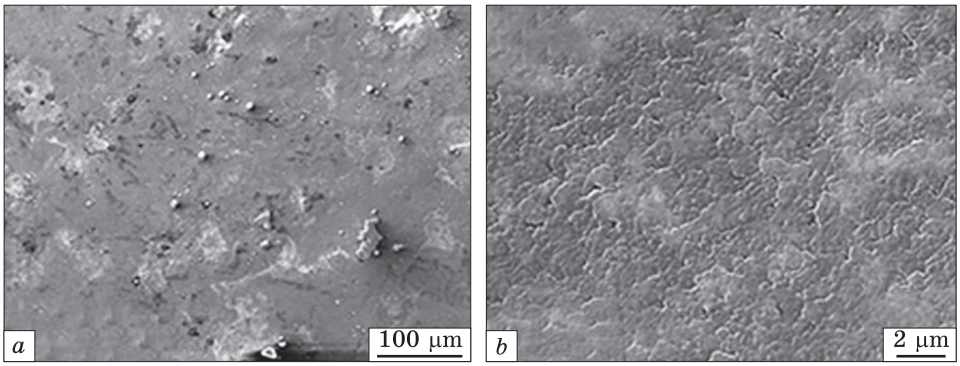

Fig. 19. SEM images of modified surface of silumin processed within the framework of conditions of variant 3

on an aluminium crystal lattice. The interlayers dividing the crystallization cells contain the particles of silicon.

Electron microscopic image of the particles having the four-petal rosettes shape is presented in Fig. 18. By the methods of dark-field analysis, it has been shown that these particles are α-titanium.

Thus, as a result of the performed studies, it has been shown that the multielemental multiphase layer ≈80 μm thick having submicro–nanocrystalline structure is formed as a result of silumin complex treatment. The presence of the droplets enriched by yttrium atoms being in the amorphous state has been detected on the surface of modification. As shown, the high-velocity crystallization of the alloyed surface layer is accompanied by the formation of α-titanium particles in the shape of cuboids and four-petal rosettes.

3.2.3. Variant 3: EEA (mode 1) + EBP (E_s = 35 J/cm²)

The characteristic electron microscopic image of silumin surface structure subjected to the combined treatment is presented in Fig. 19. It is clearly seen that the relief surface containing the regions being distinguished by contrast (Fig. 19, *a*) is formed as a result of complex treatment. The latter may be indicative of the heterogeneity of the elemental composition of the material's surface layer. The formed surface layer has the submicrocrystalline structure with crystallites' sizes less than 1 μm (Fig. 19, *b*).

The results of the studies carried by the methods of micro-x-ray spectral analysis have shown that in the surface layer of silumin, the average concentration of yttrium is 8.3 wt.% (Fig. 20).

Analysing the results of transverse metallographic sections presented in Fig. 21, we have to note that the thickness of the modified layer varies within the range of 45–80 μm. The modified layer has submicro–

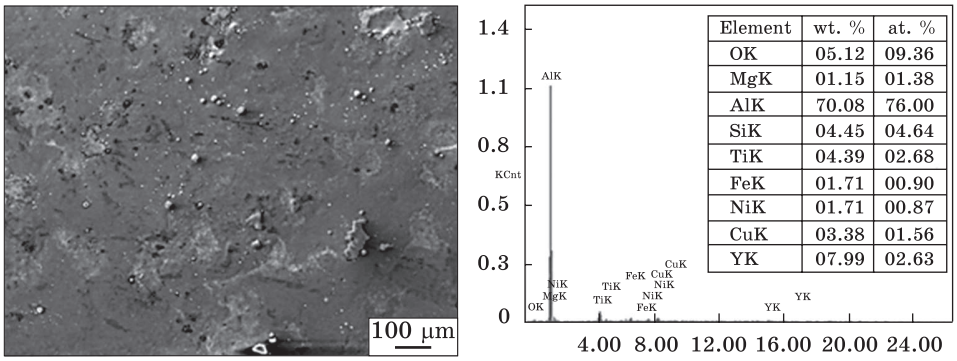

Element	wt. %	at. %
OK	05.12	09.36
MgK	01.15	01.38
AlK	70.08	76.00
SiK	04.45	04.64
TiK	04.39	02.68
FeK	01.71	00.90
NiK	01.71	00.87
CuK	03.38	01.56
YK	07.99	02.63

a *b*

Fig. 20. Structure (*a*) and corresponding energy spectra (*b*) obtained by micro-x-ray spectral analysis

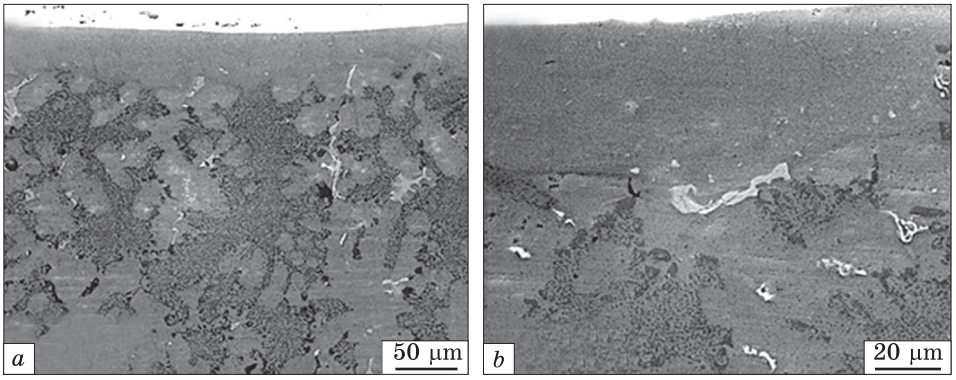

Fig. 21. Characteristic electron microscopic image of transverse metallographic section structure subjected to combined treatment (variant 3)

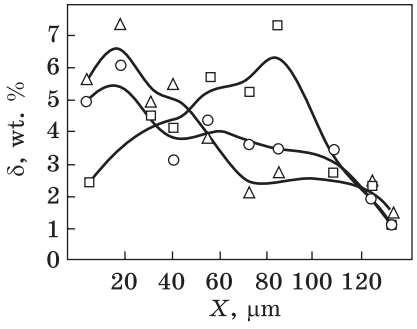

Fig. 22. Thickness distribution of relative content of Y atoms in the modified layer of silumin. The results are obtained *via* averaging of data detected by three tracks of elemental analysis

nanocrystalline structure and is free from the inclusions of silicon and intermetallides being present in silumin under study.

Results of yttrium atoms' distribution over thickness of the modified layer are presented in Fig. 22. They show that concentration profile

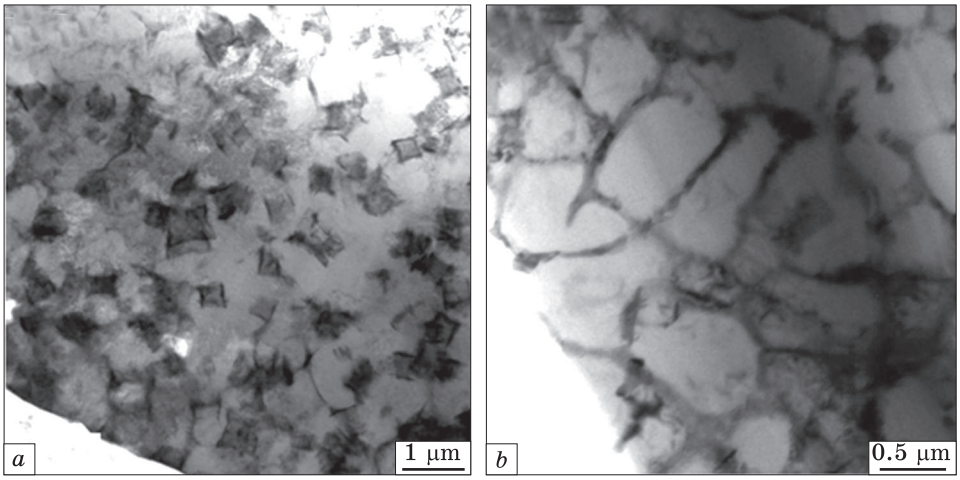

Fig. 23. TEDM image of the structure of silumin subjected to complex processing (variant 3); *a* — surface layer structure; *b* — structure of the layer located at a depth of 20–30 μm

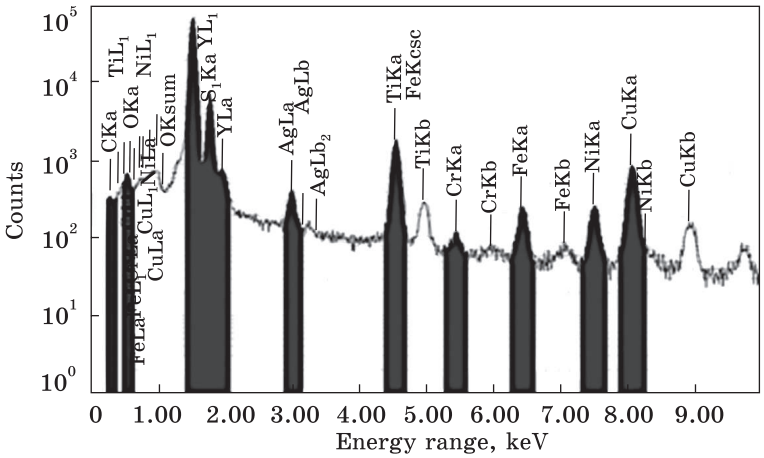

Fig. 24. Energy spectra obtained by the method of micro-x-ray spectral analysis of silumin surface layer

has a maximum, the position of which depends on the sample's region being analysed at the performed combined treatment.

Analysis of concentration profiles presented in Fig. 22 is indicative of the fact that the inhomogeneity of yttrium atoms' distribution is detected in both the transverse and the longitudinal cross-section of the material, *i.e.* it has the bulk character.

The application of the methods of transmission electron-diffraction microscopy enabled one to detect the formation of gradient submicro–

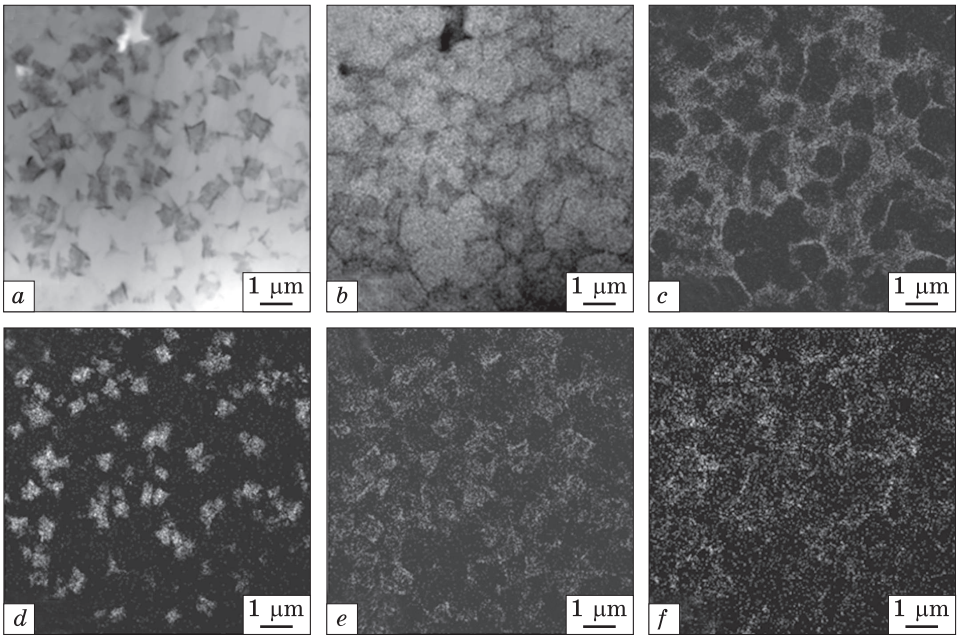

Fig. 25. Electron microscopic image of the structure of alloyed silumin layer (*a*), where images *b*–*f* are obtained through characteristic x-ray radiation of Al (*b*), Si (*c*), Ti (*d*), Y (*e*), and Cu (*f*) atoms

Table 6. **Micro-x-ray spectral analysis results of elemental composition of silumin surface layer according to energy spectra data in Fig. 24**

Thin film	Standardless	Standardless	Quantitative analysis		
Fitting coefficient: 0.1562			counts	error, %	at.%
Element, spectral line	keV	mas.%			
C, *K*					
O, *K*	0.525	0.58	2635.55	0.43	1.04
Al, *K*	1.486	79.97	638973.88	0.00	85.77
Si, *K*	1.739	7.29	60603.17	0.04	7.52
Ti, *K*	4.508	3.77	23689.20	0.09	2.28
Cr, *K*	5.411	0.11	640.12	3.62	0.06
Fe, *K*	6.398	0.61	3193.95	0.68	0.32
Ni, *K*	7.471	0.75	3484.12	0.69	0.37
Cu, *K*	8.040	3.41	13998.93	0.18	1.55
Y, *L*	1.922	2.64	5471.45	0.49	0.86
Ag, *L*	2.984	0.88	1959.87	1.02	0.24
Total		100.00			100.00

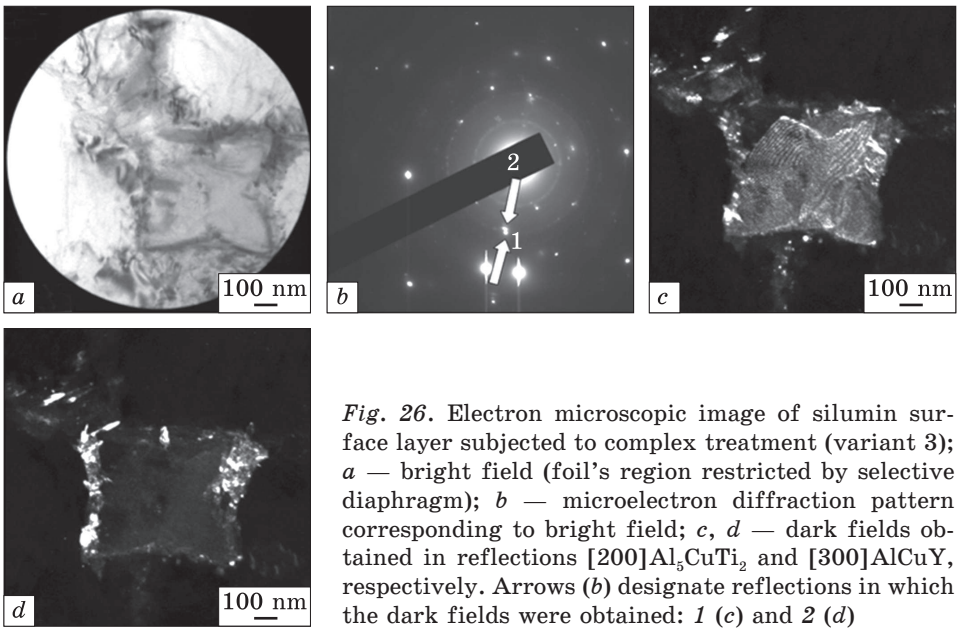

Fig. 26. Electron microscopic image of silumin surface layer subjected to complex treatment (variant 3); *a* — bright field (foil's region restricted by selective diaphragm); *b* — microelectron diffraction pattern corresponding to bright field; *c*, *d* — dark fields obtained in reflections [200]Al_5CuTi_2 and [300]AlCuY, respectively. Arrows (*b*) designate reflections in which the dark fields were obtained: *1* (*c*) and *2* (*d*)

nanoscale structure, the characteristic image of which is presented in Fig. 23 in the modified layer.

It has been determined that the modified layer up to 70 μm thick has the high-velocity cellular crystallization structure. The cells' sizes vary within the range 0.5–1.2 μm. The cells are separated by the interlayers of the second phase (Fig. 23, *b*). The inclusions of the faceted shape (Fig. 23, *a*, dark colour inclusions), whose sizes vary within the range 0.4–0.8 μm are present in the surface layer structure. The relative content of such inclusions decreases as we move away from the surface of modification.

Energy spectra obtained by the methods of micro-x-ray spectral analysis of thin foils from the surface modified layer are shown in Fig. 24. The results of the quantitative analysis of elemental composition are listed in Table 6.

The analysis of the results in Table 6 show that silumin surface layer is a multicomponent and, along with the atoms of the initial material (aluminium, silicon, copper, nickel, chromium, iron), it is additionally enriched with atoms of titanium, yttrium, and oxygen.

The method of mapping [50] enables one to analyse the distribution of the alloying elements in the volume of the material under study. The results of mapping of the surface layer of modified silumin are presented in Fig. 25.

As seen, the high-velocity crystallization cells are enriched mainly with aluminium atoms (Fig. 25, *b*). The interlayers enriched mainly

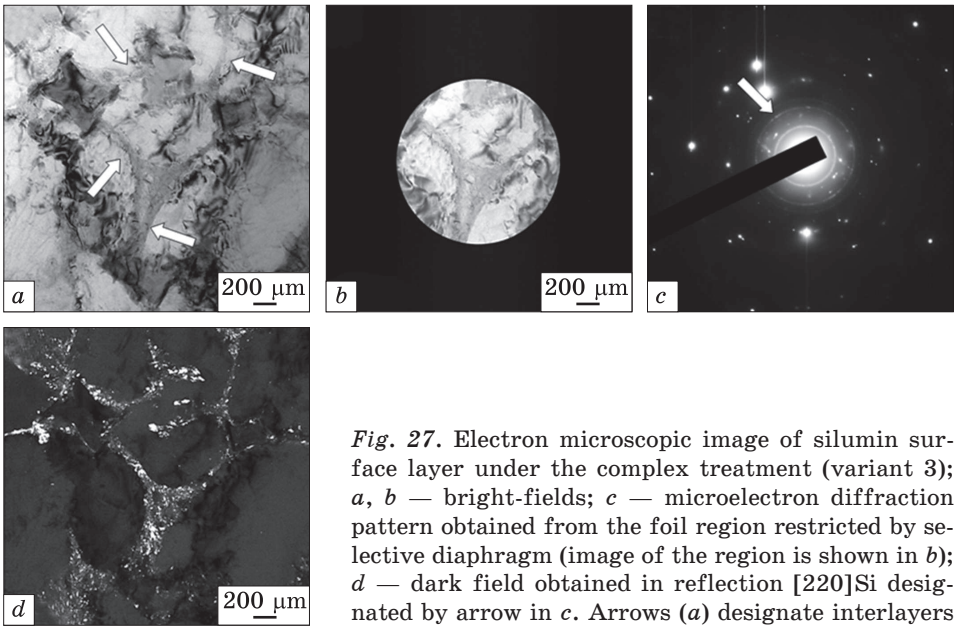

Fig. 27. Electron microscopic image of silumin surface layer under the complex treatment (variant 3); *a*, *b* — bright-fields; *c* — microelectron diffraction pattern obtained from the foil region restricted by selective diaphragm (image of the region is shown in *b*); *d* — dark field obtained in reflection [220]Si designated by arrow in *c*. Arrows (*a*) designate interlayers

with Si atoms (Fig. 25, *c*) separate the cells. The inclusions of faceted shape (Fig. 25, *a*, inclusions of dark colour) are enriched, chiefly, by atoms of titanium, aluminium, and copper (Fig. 25, *c*, *d*, *f*), the atoms of yttrium form, principally, the interlayers at the boundaries of faceted shape inclusions (Fig. 25, *e*).

Figure 26 presents the results of phase composition analysis of the surface layer of foil's region containing the faceted shape inclusions. The techniques based on obtaining the dark-field images and the method of microelectron diffraction pattern indexing [43–45, 51, 52] were used.

The performed electron microscopic microdiffraction analysis shows that faceted-shape inclusions are formed by Al_5CuTi_2 phase (Fig. 26, *c*). The interlayers of AlCuY phase composition (Fig. 26, *d*) are detected along the boundaries of these inclusions.

Figure 27 shows the characteristic image of silumin cellular crystallization structure. Microelectron diffraction pattern obtained from the given foil's region contains the separately located point reflections and the reflections forming the rings (Fig. 27, *c*). Indexing of microelectron diffraction pattern has shown that the reflections forming the diffraction rings belong to the crystal lattice of silicon. The dark-field image of silumin surface layer structure obtained in the reflection of diffraction ring (Fig. 27, *c*, reflections are designated by arrows) is shown in Fig. 27, *d*. When analysing the results presented in Fig. 27, *d*, it may be noted that silicon interlayers being located along the boundaries and boundary junction of crystallization cells formed by the solid solution

based on aluminium have a nanocrystalline structure with crystallite sizes varying within the limits of 10–20 nm.

Thus, the complex treatment of silumin surface in the mode of variant 3 resulted in the cardinal transformation of surface layer structure of the material ≈70 μm thick consisting in the dissolution of silicon inclusions and intermetallides characteristic of cast silumin and the formation of gradient multielemental submicro–nanoscale structure. It has been determined that the modified layer has the high-velocity cellular crystallization structure and contains the faceted-shape inclusions whose relative content decreases when moving away from the surface of modification. By the methods of micro-x-ray spectral analysis, it has been shown that silumin surface layer is a multielemental and, along with the atoms of the initial material (Al, Si, Cu, Ni, Cr, Fe), it is additionally enriched by Ti, Y, and O atoms. It has been established that the high-velocity crystallization cells are mainly enriched with Al atoms. The interlayer separating cells are enriched mainly with Si atoms. The faceted-shape inclusions are enriched chiefly with Ti, Al, and Cu atoms. The Y atoms form principally the interlayers along the boundaries of the faceted-shape inclusions. It has been identified that silicon interlayers (located along the boundaries and boundary junctions of crystallization cells formed by the Al-based solid solution) have the nanocrystalline structure with crystallite's sizes varying within the range of 10–20 nm.

3.2.4. Variant 4: EEA (mode 2) + EBP (E_s = 35 J/cm^2)

The characteristic electron microscopic image of silumin surface structure subjected to the combined treatment according to variant 4 is shown in Fig. 28. The fragmentation of the surface layer by microcracks is observed, the micropores, microcraters, burrs of the material are detected on the modified surface (Fig. 28, *a*). The surface layer microstructure is formed by the crystallites with size of 0.4–0.7 μm (Fig. 28, *b*).

The results of the studies performed by the methods of micro-x-ray spectral analysis have shown that the average concentrations of Y, Ti, and O atoms are 17.9, 22.5, and 6.3 wt.%, respectively.

Analysing the results of the transverse metallographic section studies presented in Fig. 29, *a*, we have to note that the thickness of the modified layer varies within the range 45–80 μm. The modified layer has a submicro–nanocrystalline structure and is free from the silicon inclusions and intermetallides present in the cast silumin (Fig. 29, *b*).

The studies of yttrium distribution over the thickness of the modified layer were carried out by the methods of micro-x-ray spectral analysis. The results (presented in Fig. 30) show that two maximums of yttrium distribution in the bulk of the modified layer are revealed. The

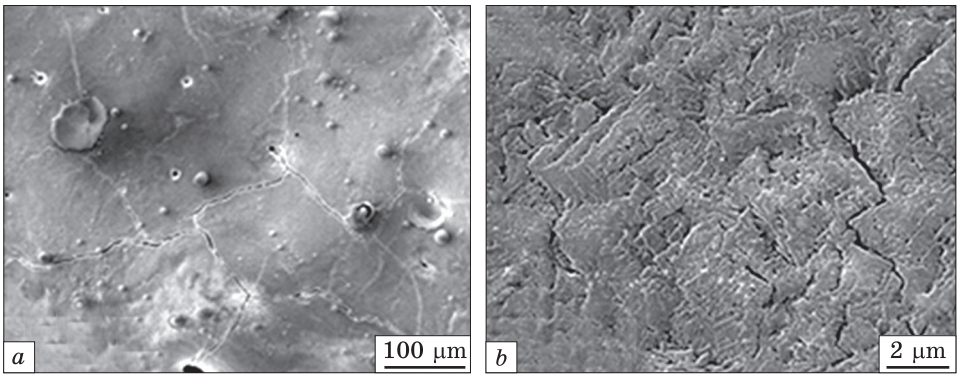

Fig. 28. SEM image of the modified surface of silumin

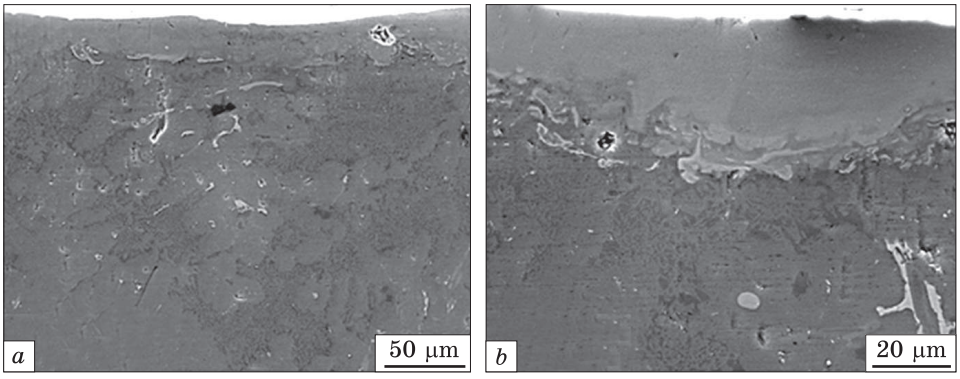

Fig. 29. Characteristic electron microscopic image of the structure of transverse metallographic section of silumin subjected to combined treatment

second maximum is often corresponds to the 'interface' between the modified layer and bulk of the silumin.

The concentration of yttrium depends on the region of the material being analysed. The analysis of concentration profiles shown in Fig. 30 is indicative of the fact that inhomogeneity of yttrium distribution is detected both in the transverse and longitudinal cross-section of the material, *i.e.* it indicates a bulk character.

The results of micro-x-ray spectral analysis of the elemental composition of silumin foil modified by the complex method are presented in Fig. 31. It is clearly seen that the thickness of the alloyed layer that is the layer wherein the presence of the alloying elements (titanium, yttrium, oxygen) are detected is less than 170 μm. The principal elements of the layer are aluminium and titanium. The concentration of other elements varies within the range 1–5 wt.%. As the distance from the surface of modification increases, the relative content of titanium and yttrium decreases, the concentration of aluminium and silicon atoms

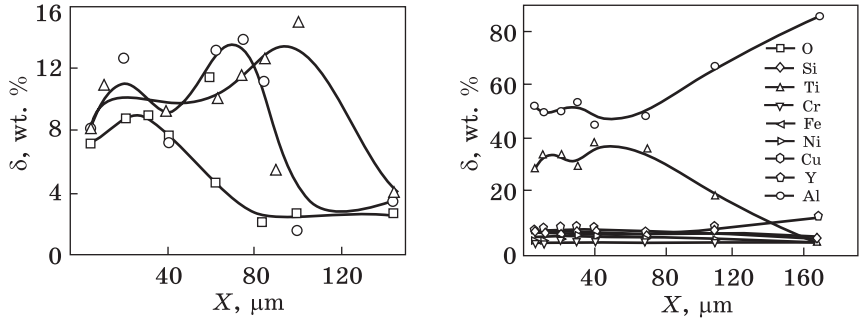

Fig. 30. Distribution of relative content of Y atoms in the thickness of silumin modified layer. The results are obtained for three tracks of elemental analysis

Fig. 31. Dependence of relative content of chemical elements on distance from surface of modification of АК10М2Н-type silumin

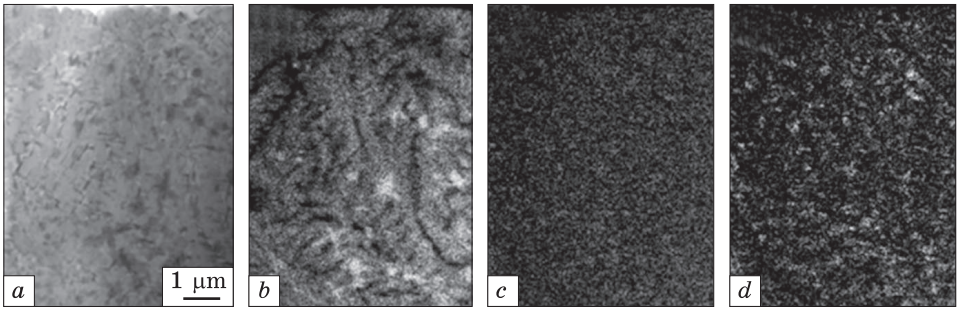

Fig. 32. Electron microscopic (bright field) image of the modified silumin layer adjoining to surface of treatment (*a*), where upper part of image corresponds to surface of modification); *b*–*d* — images of the given foil area obtained in the characteristic x-ray radiation of Ti (*b*), Si (*c*), and Y (*d*) atoms

increases reaching the values typical for silumin chemical composition, the concentration of other alloying elements varies insignificantly.

The micro-x-ray spectral analysis, namely, the method of mapping [50] enables one to visualize the distribution of the chemical elements of the modified layer of silumin sample. Figure 32 shows the results of the investigation into the distribution of titanium, silicon and yttrium atoms in the layer ≈10 μm thick adjoining to the surface of the complex treatment. As seen, the atoms of these elements are distributed nonuniformly in the surface layer forming the inclusions of different shapes and sizes. It should be stressed that the similar structure is observed up to 40 μm thick in the layer.

The quantitative analysis data of elemental composition of foil's region shown in Fig. 32, *a*, are listed in Table 7.

The layer of the material containing the particles of spherical shape enriched by Y and O atoms (Fig. 33, the particles are designated by the

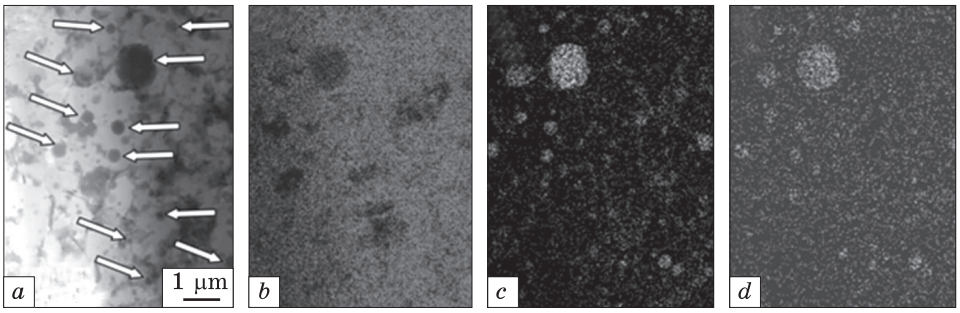

Fig. 33. Electron microscopic bright-field image of silumin layer located at distance of 40–50 μm from surface of complex treatment (variant 4) (*a*); *b*–*d* — images of the foil region obtained in characteristic x-ray radiation of Al (*b*), Y (*c*), and O (*d*) atoms. Arrows designate yttrium oxide particles

arrows) is revealed at a distance of 40–50 μm from the surface of the complex treatment. The shape of the particles and their elemental composition enable to suggest that these particles are those of yttrium oxide powder being non-destructive on electroexplosion alloying. The particle sizes vary in the range 50–1.2 μm. The results of micro-x-ray spectral quantitative analysis of this foil's region are contained in Table 8.

Figure 34 shows the results of microdiffraction electron microscopic analysis of silumin surface layer (the surface of modification is designated by the arrow in Fig. 34, *a*). It is seen that the sizes of crystallites forming the layer of the material under study vary within the ranges from units to hundreds of nanometers, *i.e.* the modified layer is a submicro–nanocrystalline material. The micro-x-ray spectral analysis of

Table 7. **Micro-x-ray spectral analysis data for foil's area in Fig. 32, *a***

Thin film	Standardless	Standardless	Quantitative analysis		
Fitting coefficient: 0.1562			counts	error, %	at.%
Element, spectral line	keV	mas.%			
O, K^*	0.525	0.83	4759.30	0.21	1.76
Al, K^*	1.486	52.18	522644.22	0.00	65.51
Si, K	1.739	4.87	50679.33	0.04	5.87
Ti, K^*	4.508	28.13	221575.55	0.01	19.89
Cr, K^*	5.411	0.26	1928.45	1.07	0.17
Fe, K^*	6.398	2.76	18118.30	0.11	1.67
Ni, K^*	7.471	0.94	5498.00	0.39	0.54
Cu, K	8.040	5.04	25938.31	0.09	2.68
Y, L^*	1.922	4.99	12964.07	0.19	1.90
Total		100.00			100.00

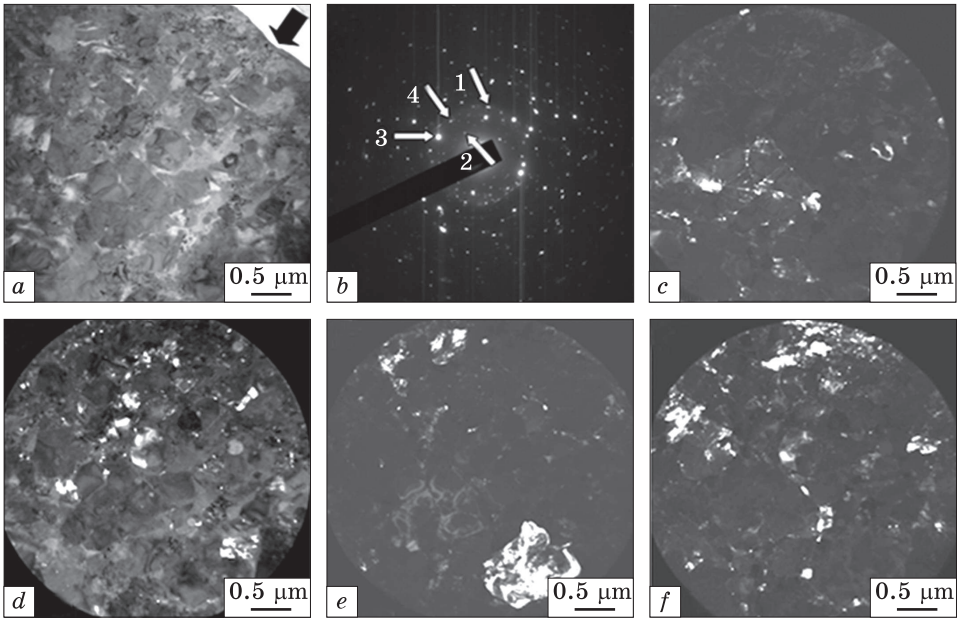

Fig. 34. Electron microscopic image of the layer adjoining to the modified silumin surface: *a* — bright field; *b* — microelectron diffraction pattern; *c* –*f* — dark fields obtained in reflections [004]$TiSi_2$ (*c*) [002]Y_3Al_2 (*d*), [111]Al (*e*), and [118]Al_3Ti (*f*). Arrows designate surface of modification (*a*) and reflections in which dark fields were obtained (*b*): *1* — *c*, *2* — *d*, *3* — *e*, *4* — *f*

Table 8. **Results of micro-x-ray spectral analysis of foil's region presented in Fig. 33, *a***

Thin film	Standardless	Standardless	Quantitative analysis		
Fitting coefficient: 0.1562			counts	error, %	at.%
Element, spectral line	keV	mas.%			
O, *K*	0.525	0.87	2498.31	0.23	1.91
Al, *K*	1.486	45.17	227359.34	0.00	59.15
Si, *K*	1.739	3.34	17460.58	0.06	4.20
Ti, *K*	4.508	38.24	151318.00	0.01	28.20
Cr, *K*	5.411	0.29	1058.59	1.12	0.20
Fe, *K*	6.398	2.36	7804.34	0.14	1.50
Ni, *K*	7.471	0.82	2406.36	0.51	0.49
Cu, *K*	8.040	5.10	13192.37	0.10	2.83
Y, *L*	1.922	3.82	4985.79	0.28	1.52
Total		100.00			100.00

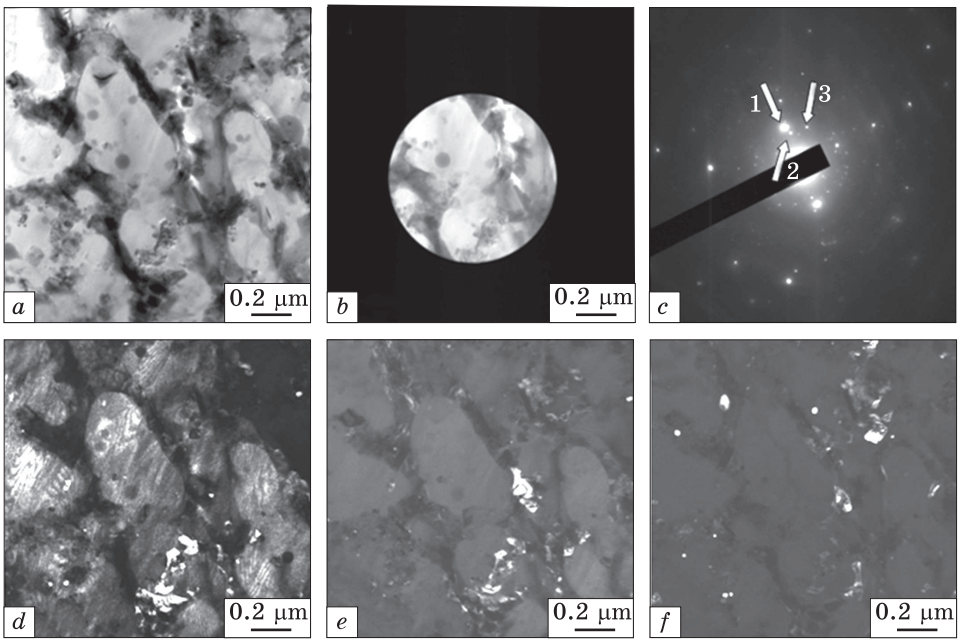

Fig. 35. Electron microscopic image of the layer located at a distance of ≈70 μm from the modified surface: *a*, *b* — bright fields; *c* — microelectron diffraction pattern; *d*–*f* — dark fields obtained in reflections [111]Al + [302]Si (*d*), [111]Si (*e*), [111]$Cu_{2.7}Fe_{6.3}Si$ (*f*). Arrows (*c*) designate reflections in which dark fields were obtained *1* — *d*, *2* — *e*, *3* — *f*

the surface layer of the modified material has shown that the principal chemical elements of the layer Al, Ti, Si, Cu, and Y (Fig. 32, Table 7) are contained in a substantially lesser amount. The results of the dark-field analysis of phase composition of this layer are presented in Fig. 34, *c*–*f*. The microelectron-diffraction pattern analysis shows that the crystallites of submicron sizes are formed by the Al-based solid solution (Fig. 34, *e*). The inclusions of nanoscale range are formed by the particles of titanium and yttrium aluminides (Al_3Ti and Y_3Al_2) as well as titanium silicides ($TiSi_2$).

The results of microdiffraction electron microscopic analysis of the layer located at a distance of ≈70 μm are presented in Fig. 35.

It is clearly seen that at the given distance from the surface of modification the silumin structure is presented by the cells of high-velocity crystallization. The cells' sizes vary within the range of 0.5–0.6 μm. The microelectron diffraction-pattern analysis (Fig. 35, *c*) shows that the cells of crystallization are formed by the Al-based solid solution (Fig. 35, *d*). The cells are separated by the interlayers of the second phase, the transverse sizes of which vary from of 50 to 70 nm. The microdiffraction analysis with the usage of the dark-field image tech-

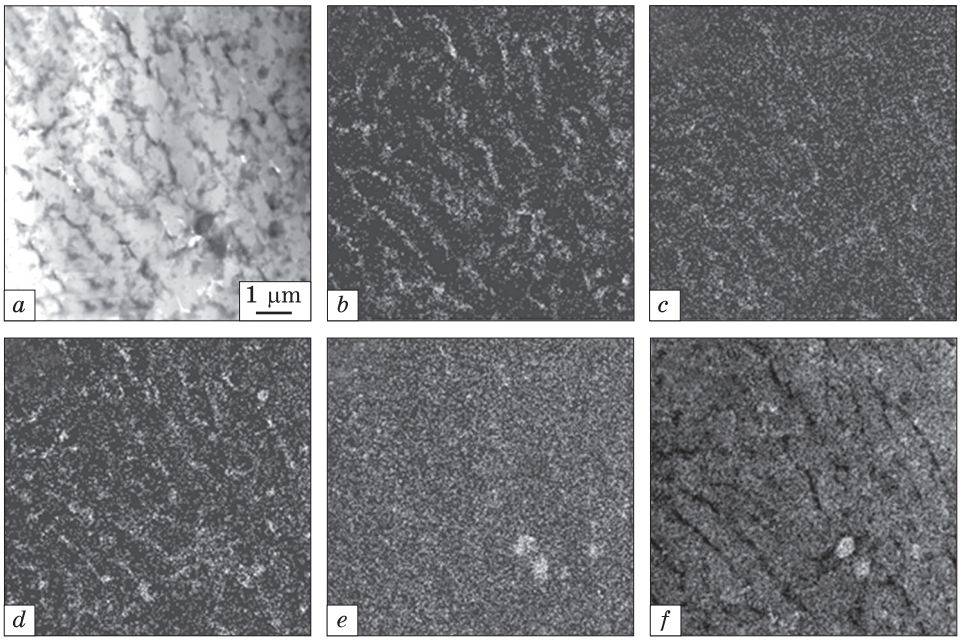

Fig. 36. Electron microscopic bright-field image of silumin layer located at a distance of ≈70 μm from the surface of complex treatment (*a*); *b*–*f* — images of the foil area obtained through characteristic x-ray of Fe (*b*), Cu (*c*), Y (*d*), Si (*e*), and Ti (*f*) atoms

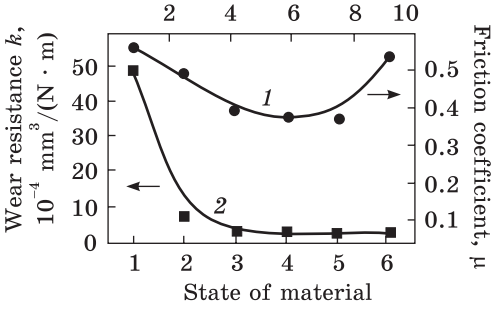

Fig. 37. Friction coefficient, μ, (curve *1*) and wear resistance parameter, *k*, (curve *2*) *vs*. the state of silumin samples: 1 — cast state, 2 —state after irradiation by EBP, 3–6 — states after treatment combining the electroexplosion alloying and irradiation by intense pulsed electron beam (3 — variant 1, 4 — variant 2, 5 — variant 3, and 6 — variant 4)

nique shows that the particles of silicon (Fig. 35, *d*, *e*) and the particles of $Cu_{2.7}Fe_{6.3}Si$ compound (Fig. 35, *f*) are located at the boundaries of crystallization cells. The results of micro-x-ray spectrum analysis presented in Fig. 36 support the possibility of interlayer's formation of the given elemental composition.

Thus, the studies carried out by the methods of scanning and transmission electron diffraction microscopy show that the thickness of the alloyed layer, *i.e.* the layer wherein the presence of the alloying elements (Ti, Y, O) is detected, reaches ≈170 μm. The main elements of the alloyed layer are Al and Ti. By the method of mapping, the inhomo-

geneous distribution of alloying atoms in the modified layer has been identified. As shown, the electroexplosion processing is accompanied with both the alloying of the surface layer with elements of plasma and the penetration of initial powder particles of yttrium oxide into the surface layer. As established, the complex treatment results in the formation of the multiphase submicro–nanoscale state, where the sizes of crystallites vary from several to hundreds of nanometers in silumin surface layer.

3.3. Wear Resistance

The detected transformations of silumin surface layer should have a substantial effect on the tribological properties of the material. The performed tests, the results of which are presented in Fig. 37, showed that the complex surface treatment of silumin results in multiple increase in wear resistance of the modified layer and decrease in friction coefficient, *i.e.* caused by the formation of the multiphase submicro–nanocrystalline state.

Wear parameter (the value inverse to wear resistance of the material) depends strongly on the variant of the combined treatment. With respect to the initial silumin, the 18–20-fold increase of the wear resistance was detected; in relation to silumin irradiated by intense pulsed electron beam, the 2.6–2.8-fold increase of the wear resistance was determined. The friction coefficient is lesser pronounced: it decreases by ≈1.5 times at the combined treatments (variants 1–3) with respect to the initial silumin and by ≈1.3 times with respect to silumin irradiated by intense pulsed electron beam. In case of the 4-th variant of the combined treatment, the friction coefficient increases and reaches the value close to that for the initial silumin.

4. Conclusion

The complex treatment of hypoeutectic silumin surface combining the electroexplosion alloying with titanium and yttrium oxide and the subsequent irradiation by intense pulsed electron beam was realized. The investigations carried out by the methods of state-of-the-art physical materials science have revealed the formation of the extended surface layer wherein the concentration of titanium and yttrium depends on the regime (mode) of electroexplosion alloying and on the distance to the surface modification. By the method of mapping, the inhomogeneous distribution of alloying atoms in the modified layer was detected. As established, the electroexplosion processing is accompanied with both the alloying of the surface layer with elements of plasma and the penetration of the initial powder particles of yttrium oxide into the surface layer. It was determined that the combined treatment results in the for-

mation of the multiphase submicro–nanoscale state, where the sizes of crystallites vary several to hundreds of nanometers in silumin surface layer. As shown, the wear resistance of the material depends on the variant of the combined treatment. With respect to the initial silumin, the wear resistance is 18–20-fold increased; in relation to silumin irradiated by intense pulsed electron beam, the wear resistance is increased by 2.6–2.8 times. The friction coefficient varies less pronouncedly: it decreases by ≈1.5 times and corresponds to variants 1–3 of the combined treatment with respect to the initial silumin, and it decreases by ≈1.3 times with respect to the silumin irradiated by intense pulsed electron beam. Under the condition of combined treatment, with corresponds to variant 4, the friction coefficient of the modified layer is close to the value found for the silumin before the processing, *i.e.* in its initial state.

Acknowledgments. The investigations were supported financially by the Ministry of Science and Education of RF (project no. 3.1283.2017/4.6), and grants of RFFI (projects nos. 19-52-04009 and 19-48-700010).

REFERENCES

1. V.E. Gromov, S.V. Konovalov, K.V. Aksenova, and T.Yu. Kobzareva, *Ehvolutsiya Struktury i Svoistv Legkikh Splavov pri Ehnergeticheskikh Vozdeistviyakh* [Evolution of Structure and Properties of Light Alloys under Energy Impacts] (Novosibirsk: SB RAS: 2016) (in Russian).
2. A.Ya. Bagautdinov, E.A. Budovskikh, Yu.F. Ivanov, and V.E. Gromov, *Fizicheskie Osnovy Ehlektrovzryvnogo Legirovaniya Metallov i Splavov* [Physical Fundamentals of Electroexplosion Alloying of Metals and Alloys] (Novokuznetsk: SibSIU: 2007) (in Russian).
3. V.E. Gromov, Yu.F. Ivanov, S.E. Vorobiev, and S.V. Konovalov, *Fatigue of Steels Modified by High Intensity Electron Beams* (Cambridge: 2015).
4. Yu.F. Ivanov, V.E. Gromov, S.V. Konovalov, and S. Chen, *Fundamental'nyye Problemy Sovremennogo Materialovedeniya*, **15**, No. 4: 506 (2018). https://doi.org/10.25712/ASTU.1811-1416.2018.04.009
5. D.V. Zagulyaev, V.E. Gromov, Yu.F. Ivanov, E.A. Petrikova, A.D. Teresov, S.V. Konovalov, and A.P. Semin, *J. Phys.: Conf. Ser.*, **1115**: 032021 (2018). https://doi.org/10.1088/1742-6596/1115/3/032021
6. V.V. Shlyarov, K.A. Osintsev, K.A. Butakova, D.V. Zagulyaev, and D.A. Romanov, *Promising Materials and Technologies: Int. Symposium Proc.* (2017), p. 91.
7. S. Konovalov, V. Gromov, and Yu. Ivanov, *Mater. Res. Express*, **5**: 116520 (2018). https://doi.org/10.1088/2053-1591/aadd29
8. D. Zagulyaev, S. Konovalov, V. Gromov, A. Glezer, Yu. Ivanov, and R. Sundeev, *Mater. Lett.*, **229**: 377 (2018). https://doi.org/10.1016/j.matlet.2018.07.064
9. V.E. Gromov, Yu.F. Ivanov, D.V. Zagulyaev, O.S. Tolkachev, E.A. Petrikova, and S.V. Konovalov, *IOP Conf. Ser.: Mater. Sci. Eng.*, **411**: 012023 (2018). https://doi.org/10.1088/1757-899X/411/1/012023
10. Yu.F. Ivanov, V.E. Gromov, S.V. Konovalov, D.V. Zagulyaev, E.A. Petrikova, and A.P. Semin, *Uspehi Fiziki Metallov*, **19**, No. 2: 195 (2018). https://doi.org/10.15407/ufm.19.02.195

11. Ye.A. Budovskikh, V.D. Sarychev, V.E. Gromov, P.S. Nosarev, and E.V. Martusevich, *Osnovy Tekhnologii Obrabotki Poverkhnosti Materialov Impulsnoy Geterogennoy Plazmoy* [Fundamentals of Technology of Surface Treatment of Materials by Pulsed Heterogeneous Plasma] (Novokuznetsk: SibSIU: 2002) (in Russian).
12. N.N. Koval' and Yu.F. Ivanov, *Ehvolyutsiya Struktury Poverkhnostnogo Sloya Stali, Podvergnutoy Ehlektronno-Ionno-Plazmennym Metodam Obrabotki* [Evolution of Surface Layer Structure of Steel Subjected to Electron-Ion-Plasma Methods] (Tomsk: NTL: 2016) (in Russian).
13. N.N. Koval' and Yu.F. Ivanov, *Ehlektronno-Ionno-Plazmennaya Modifikatsiya Poverkhnosti Tsvetnykh Metallov i Splavov* [Electron-Ion-Plasma Modification of Surface of Non-Ferrous Metals and Alloys] (Tomsk: NTL: 2016) (in Russian).
14. Y. Hao, B. Gao, G.F. Tu, H. Cao, S.Z. Hao, and C. Dong, *Appl. Surf. Sci.*, **258**, No. 6: 2052 (2012). https://doi.org/10.1016/j.apsusc.2011.04.104
15. B. Gao, Y. Hao, Z. Wang, G.F. Tu, W.X. Shi, S.W. Li, S.Z. Hao, and C. Dong, *Trans. Mater. Heat Treatment*, No. 3: 135 (2010).
16. B. Gao, Y. Hao, W.F. Zhuang, G.F. Tu, W.X. Shi, S.W. Li, S.Z. Hao. C. Dong, and M.C. Li, *Phys. Proc.*, **18**: 187 (2011). https://doi.org/10.1016/j.phpro.2011.06.079
17. Y. Hao, B. Gao, G.F. Tu, S.W. Li, and C. Dong, *Nucl. Instrum. Methods Phys. Res. B*, **269**, No. 13: 1499 (2011). https://doi.org/10.1016/j.nimb.2011.04.010
18. Y. Hao, B. Gao, G.F. Tu, S.W. Li, S.Z. Hao, and C. Dong, *Appl. Surf. Sci.*, **257**, No. 9: 3913 (2011). https://doi.org/10.1016/j.apsusc.2010.11.118
19. Y. Hao, B. Gao, G. F. Tu, S. W. Li, S. Z. Hao, and C. Dong, *Trans. Mater. Heat Treatment*, No. 9: 115 (2010).
20. Y. Hao, B. Gao, G.F. Tu, Z. Wang, and C.Z. Hao, *Mater. Sci. Forum.*, **675–677**: 693 (2011). https://doi.org/10.4028/www.scientific.net/MSF.675-677.693
21. J. An, X.X. Shen, Y. Lu, Y.B. Liu, R.G. Li, C.M. Chen, and M.J. Zhang, *Surf. Coat. Technol.*, **200**, No.: 18-19: 5590 (2006). https://doi.org/10.1016/j.surfcoat.2005.07.106
22. J. An, X.X. Shen, and Y. Lu, *Wear*, **261**, No. 2: 208 (2006). https://doi.org/10.1016/j.wear.2005.09.014
23. S. Hao, S. Yao, J. Guan, A. Wu, P. Zhong, and C. Dong, *Curr. Appl. Phys.*, **1**, Nos. 2–3: 203. (2001). https://doi.org/10.1016/S1567-1739(01)00017-7
24. T. Grosdidier, J.X. Zou, N. Stein, C. Boulanger, S.Z. Hao, and C. Dong, *Scripta Mater.*, **58**, No. 12: 1058 (2008). https://doi.org/10.1016/j.scriptamat.2008.01.052
25. Yu.F. Ivanov, V.E. Gromov, S.V. Konovalov, D.V. Zagulyaev, and E.A. Petrikova, *Russian Metallurgy (Metally)*, **2019**, No. 4: 398 (2019). https://doi.org/10.1134/S0036029519040189
26. D. Zagulyaev, S. Konovalov, V. Gromov, A. Melnikov, and V. Shlyarov, *Bulletin of the Polish Academy of Sciences: Technical Sciences*, **67**, No. 2: 173 (2019). https://doi.org/10.24425/bpas.2019.128605
27. D.V. Zagulyaev, V.E. Gromov, S.V. Konovalov and Yu.F. Ivanov, *Inorganic Mater.: Appl. Res.*, **10**, No. 3: 622 (2019). https://doi.org/10.1134/S2075113319030432

28. V. Gromov, S. Konovalov, Y. Ivanov, D. Zaguliaev, E. Petrikova, and Y. Serenkov, *Mater. Res. Express*, **6**, No. 7: 076574 (2019). https://doi.org/10.1088/2053-1591/ab1683
29. S. Konovalov, V. Gromov, D. Zaguliyaev, Y. Ivanov, A. Semin, and J. Rubannikova, *Archives of Foundry Engineering*, **19**, No. 2: 79 (2019).
30. Yu.F. Ivanov, S.V. Karpii, M.M. Morozov, N.N. Koval', E.A. Budovskikh, and V.E. Gromov, *Struktura, Fazovyi Sostav i Svoystva Titana Posle Ehlektrovzryvnogo Legirovaniya i Ehlektronno-Puchkovoy Obrabotki* [Structure, Phase Composition and Properties of Titanium after Electroexplosive Alloying and Electron-Beam Processing] (Novokuznetsk: Publishing House NPK: 2010) (in Russian).
31. E.A. Budovskikh, E.S. Vashchuk, V.E. Gromov, Yu.F. Ivanov, and N.N. Koval' *Formirovanie Strukturno-Fazovykh Sostoyaniy Metallov i Splavov pri Ehlektrovzryvnom Legirovanii i Ehlektronno-Puchkovoy Obrabotke* [Formation of Structural-Phase States of Metals and Alloys at Electroexplosion Doping and Electron-Beam Processing] (Novokuznetsk: Inter-Kuzbass: 2011) (in Russian).
32. V.E. Gromov, K.V. Sosnin, Yu.F. Ivanov, and O.A. Semina, *Uspehi Fiziki Metallov*, **16**, No. 3: 175 (2015) (in Russian). https://doi.org/10.15407/ufm.16.03.175
33. V.E. Gromov, Yu.F. Ivanov, O.A. Peregudov, K.V. Morozov, and A.P. Semin, *Uspehi Fiziki Metallov*, **17**, No. 3: 253 (2016) (in Russian). https://doi.org/10.15407/ufm.17.03.253
34. K.V. Sosnin, V.E. Gromov, and Yu.F. Ivanov, *Struktura i Fazovyi Sostav Titana posle Ehlektrovzryvnogo Legirovaniya Ittriem i Ehlektronno-Luchevoy Obrabotki* [Structure and Phase Composition of Titanium after Electro-Explosive Alloying by Yttrium and Electron Beam Processing] (Novokuznetsk: Poligrafist: 2015) (in Russian).
35. V.F. Terekhova and E.M. Savitskiy, *Ittriy* [Yttrium] (Moscow: Science: 1967) (in Russian).
36. A.E. Vol and I.K. Kagan, *Struktura i Svoistva Dvoinykh Metallicheskikh Sistem* [The Structure and Properties of Binary Metal Systems] (Moscow: Science: 1976) (in Russian).
37. *Splavy Alyuminievyye dlya Proizvodstva Porshney* [Aluminium Alloys for Manufacturing of Plungers] (GOST 30620-98) (Minsk: Interstate Committee on Standardization, Metrology and Certification: 2000) (in Russian).
38. N.N. Koval' and Yu.F. Ivanov, *Russ. Phys. J*, **51**, No. 5: 505 (2008). https://doi.org/10.1007/s11182-008-9073-7
39. Yu.A. Denisova, Yu.F. Ivanov, O.V. Ivanova, I.A. Ikonnikova, N.N. Koval, O.V. Krysina, E.A. Petrikova, A.D. Teresov, and V.V. Shugurov, *Strukturnaya Ehvolutsiya Poverkhnostnogo Sloya Stali, Podvergnutogo Ehlektronno-Ionno-Plazmovym Metodam Obrabotki* [Structure Evolution of Steel Surface Layer Subjected to Electron–Ion-Plasma Methods of Processing] (Tomsk: NTL: 2016) (in Russian).
40. Yu.Kh. Akhmadeev, V.V. Denisov, Yu.F. Ivanov, O.V. Ivanova, I.A. Ikonnikova, N.N. Koval', O.V. Krysina, I.V. Lopatin, E.A. Petrikova, M.S. Petyukevich, A.D. Teresov, O.S. Tolkachev, and V.V. Shugurov, *Ehlektronno-Ionno-Plazmovaya Modifikatsiya Poverkhnosti Tsvetnykh Metallov i Splavov* [Electron–Ion-Plasma Modification of Surface of Non-Ferrous Metals and Alloys] (Tomsk: NLT: 2016) (in Russian).
41. Yu.F. Ivanov, N.N. Koval, V.I. Vlasov, A.D. Teresov, E.A. Petrikova, V.V. Shugurov, O.V. Ivanova, I.A. Ikonnikova, and A.A. Klopotov, *High-Temp. Mater. Processes*, **17**, No. 4: 241 (2013). https://doi.org/10.1615/HighTempMatProc.v17.i4.60

42. Yu.F. Ivanov, O.V. Krysina, M. Rygina, E.A. Petrikova, A.D. Teresov, V.V. Shugurov, O.V. Ivanova, and I.A. Ikonnikova, *High Temp. Mater. Processes*, **18**, No. 4: 311 (2014). https://doi.org/10.1615/HighTempMatProc.2015015710
43. *Transmission Electron Microscopy Characterization of Nanomaterials* (Ed. C.S.S.R. Kumar) (New York: Springer: 2014). https://doi.org/10.1007/978-3-642-38934-4
44. D.B. Williams and C.B. Carter, *Transmission Electron Microscopy. A Textbook for Materials Science* (Boston: Springer: 2009). https://doi.org/10.1007/978-0-387-76501-3
45. R.F. Egerton, *Physical Principles of Electron Microscopy. An Introduction to TEM, SEM, and AEM* (Springer International Publishing: 2016). https://doi.org/10.1007/978-3-319-39877-8
46. L.F. Mondolfo, *Aluminum Alloys: Structure and Properties* (London: Butterworth-Heinemann: 1976). https://doi.org/10.1016/C2013-0-04239-9
47. N.A. Belov, *Fazovyy Sostav Alyuminievykh Splavov* [Phase Composition of Aluminium Alloys] (Moscow: MISiS: 2009) (in Russian).
48. M.M. Makhloufe and H.V. Guthy, *J. Light Metals*, **1**, No. 4: 199 (2001). https://doi.org/10.1016/S1471-5317(02)00003-2
49. A.P. Laskovnev, Yu.F. Ivanov, E.A. Petrikova, N.N. Koval', V.V. Uglov, N.N. Cherenda, N. V. Bibik, and V. M. Astashensky, *Modifikatsiya Struktury i Svoistv Ehvtekticheskogo Silumina Ehlektronno-Ionno-Plazmennoy Obrabotkoy* [Modification of Structure and Properties of Eutectic Silumin by Electron–Ion-Plasma Processing] (Minsk: Navuka: 2013) (in Russian).
50. D. Brandon and W.D. Kaplan, *Microstructural Characterization of Materi*als (Chichester: John Wiley & Sons Ltd.: 2008).
51. L.M. Utevskiy, *Difraktsionnaya Ehlektronnaya Mikroskopiya v Metallurgii* [Diffraction Electron Microscopy in Metallurgy] (Moscow: Metallurgiya: 1973) (in Russian).
52. K.W. Andrews, D.J. Dyson, and S.R. Keown, *Interpretation of Electron Diffraction Patterns* (New York: Springer: 1967). https://doi.org/10.1007/978-1-4899-6475-5

Received July 4, 2019;
in final version, November 8, 2019

Ю.Ф. Іванов[1], *В.Є. Громов*[2], *Д.В. Загуляєв*[2],
С.В. Коновалов[3], *Ю.А. Рубаннікова*[2], *О.П. Семін*[2]

[1] Інститут сильнострумової електроніки СВ РАН,
просп. Академічний, 2/3, 634055 Томськ, Росія
[2] Сибірський державний індустріальний університет,
вул. Кірова, 42, 654007 Новокузнецьк, Росія
[3] Самарський національний дослідницький університет
імені академіка С.П. Корольова,
Московське шосе, 34, 443086 Самара, Росія

СТРУКТУРА ТА ВЛАСТИВОСТІ ДОЕВТЕКТИЧНОГО СИЛУМІНУ, ПІДДАНОМУ КОМПЛЕКСНОМУ ЕЛЕКТРОННО-ЙОННОМУ ПЛАЗМОВОМУ ОБРОБЛЕННЮ

Методами сучасного фізичного матеріалознавства проведено пошарову аналізу структурно-фазових станів і трибологічних властивостей доевтектичного силуміну марки АК10М2Н на глибині до 170 мкм після комплексного оброблення.

Воно полягало в електропідривному леґуванні титаном і порошком оксиду ітрію в різних співвідношеннях з подальшим електронно-пучковим обробленням. Вибір титану й ітрію в якості леґувальних елементів зумовлено тим, що при твердінні вони утворюють евтектичну суміш двох обмежених твердих розчинів. В роботі реалізовано чотири варіянти комбінованого оброблення поверхні: маси підривних фолії титану та порошку Y_2O_3 становили по 58,9 мг при густині енергії пучка електронів E_s = 25 Дж/см^2 і напрузі розряду U = 2,8 кВ, а також 58,9 і 88,3 мг при E_s = 35 Дж/см^2 і U = 2,6 кВ. Встановлено, що електропідривне оброблення супроводжується як леґуванням поверхневого шару елементами плазми, так і втіленням у поверхневий шар частинок вихідного порошку оксиду ітрію. Комплексне поверхневе оброблення приводить до розчинення включень Si й інтерметалідів, характерних для литого стану. Воно, залежно від режиму, формує багатоелементний багатофазний шар товщиною до ≈170 мкм, розміри кристалітів якого змінюються в межах від одиниць до сотень нанометрів. Поряд з атомами вихідного матеріалу (Al, Si, Cu, Ni, Fe), поверхневий шар збагачено атомами Титану, Ітрію, Оксиґену. Методою катрирування виявлено неоднорідний розподіл леґувальних елементів у модифікованому шарі. Виявлено, що модифікований шар має структуру високошвидкісної коміркової кристалізації та містить включення огранованої форми, відносний вміст яких понижується в міру віддалення від поверхні. Комірки високошвидкісної кристалізації збагачено переважно атомами Al; прошарки, що розділяють комірки, збагачено переважно атомами Si; включення огранованої форми збагачено переважно атомами Ti, Al і Cu; атоми Y переважно формують прошарки по межах включень огранованої форми. Виявлено, що прошарки кремнію, розташовані уздовж меж і у стиках меж комірок кристалізації, сформованих твердим розчином на основі алюмінію, мають нанокристалічну структуру з розміром кристалітів, що змінюються у межах 10–20 нм. Комплексне поверхневе оброблення збільшує зносостійкість у 18–20 разів відносно вихідного силуміну та в 2,6–2,8 рази по відношенню до силуміну після електропідривного леґування. Коефіцієнт тертя понижується в ≈1,5 рази відносно вихідного силуміну.

Ключові слова: доевтектичний силумін, електропідривне леґування, титан, ітрій, електронно-пучкове оброблення, структура, фазовий склад, зносостійкість.

Ю.Ф. Иванов[1], *В.Е. Громов*[2], *Д.В. Загуляев*[2],
С.В. Коновалов[3], *Ю.А. Рубанникова*[2], *А.П. Семин*[2]

[1] Институт сильноточной электроники СО РАН,
просп. Академический, 2/3, 634055 Томск, Россия
[2] Сибирский государственный индустриальный университет,
ул. Кирова, 42, 654007 Новокузнецк, Россия
[3] Самарский национальный исследовательский университет
имени академика С.П. Королёва,
Московское шоссе, 34, 443086 Самара, Россия

СТРУКТУРА И СВОЙСТВА ДОЭВТЕКТИЧЕСКОГО СИЛУМИНА, ПОДВЕРГНУТОГО КОМПЛЕКСНОЙ ЭЛЕКТРОННО-ИОННОЙ ПЛАЗМЕННОЙ ОБРАБОТКЕ

Методами современного физического материаловедения проведён послойный анализ структурно-фазовых состояний и трибологических свойств доэвтектического силумина марки АК10М2Н на глубине до 170 мкм после комплексной обработки. Она заключалась в электровзрывном легировании титаном и порошком ок-

сида иттрия в разных соотношениях с последующей электронно-пучковой обработкой. Выбор титана и иттрия в качестве легирующих элементов обусловлен тем, что при затвердевании они образуют эвтектическую смесь двух ограниченных твёрдых растворов. В работе реализованы четыре варианта комбинированной обработки поверхности: массы взрываемых фольги титана и порошка Y_2O_3 составляли по 58,9 мг при плотности энергии пучка электронов E_s = 25 Дж/см^2 и напряжении разряда U = 2,8 кВ, а также 58,9 и 88,3 мг при E_s = 35 Дж/см^2 и U = 2,6 кВ. Установлено, что электровзрывная обработка сопровождается как легированием поверхностного слоя элементами плазмы, так и внедрением в поверхностный слой частиц исходного порошка оксида иттрия. Комплексная поверхностная обработка приводит к растворению включений Si и интерметаллидов, характерных для литого состояния. Она, в зависимости от режима, формирует многоэлементный многофазный слой толщиной до ≈170 мкм, размеры кристаллитов которого изменяются в пределах от единиц до сотен нанометров. Наряду с атомами исходного материала (Al, Si, Cu, Ni, Fe), поверхностный слой обогащён атомами титана, иттрия, кислорода. Методом катрирования выявлено неоднородное распределение легирующих элементов в модифицированном слое. Выявлено, что модифицированный слой имеет структуру высокоскоростной ячеистой кристаллизации и содержит включения огранённой формы, относительное содержание которых снижается по мере удаления от поверхности. Ячейки высокоскоростной кристаллизации обогащены преимущественно атомами Al; прослойки, разделяющие ячейки, обогащены преимущественно атомами Si; включения огранённой формы обогащены преимущественно атомами Ti, Al и Cu; атомы Y преимущественно формируют прослойки по границам включений огранённой формы. Выявлено, что прослойки кремния, располагающиеся вдоль границ и в стыках границ ячеек кристаллизации, сформированных твёрдым раствором на основе алюминия, имеют нанокристаллическую структуру с размером криталлитов, изменяющимся в пределах 10–20 нм. Комплексная поверхностная обработка увеличивает износостойкость в 18–20 раз по отношению к исходному силумину и в 2,6–2,8 раза по отношению к силумину после электровзрывного легирования. Коэффициент трения снижается в ≈1,5 раза по отношению к исходному силумину.

Ключевые слова: доэвтектический силумин, электровзрывное легирование, титан, иттрий, электронно-пучковая обработка, структура, фазовый состав, износостойкость.